

## **Author response to reviewers for manuscript TC-2018-56**

We are very grateful to all three reviewers for their detailed and constructive reviews of our manuscript.

Below, we have responded to each of the reviewers' comments sequentially. Here, the original reviewers' comments are in normal font and our responses are in *italicised* font. At the end of this response, we have also included an updated version of the manuscript with all of the tracked changes visible.

## Response to reviewer #1 (Allen Pope)

“Dual-satellite (Sentinel-2 and Landsat 8) remote sensing of supraglacial lakes in Greenland” by Williamson et al. explores a new method of retrieving supraglacial lake depth from Sentinel-2 imagery, combines it with Landsat 8 to build a higher-temporal resolution record, tracks lake volume/filling/draining, and investigates the impact of lakes of various size on the hydrology of the Greenland Ice sheet.

Williamson et al. have produced a paper which is clear, clean, logical, well-written, and ultimately enjoyable to read. Thoughtful consideration has been given to how to combine datasets and how to interpret the resultant data. However, there are some crucial factors that I believe the paper should consider before being published.

*We are grateful of the positive comments on our manuscript, thank you.*

Choosing the Sentinel-2 Method:

This comparison is a big step in the paper and will facilitate many future studies. However, I think there are one or two options which really need to be carefully considered before claiming victory – in particular exploring the use of the S2 Green Band. In Figure 3, evidence of saturation is clearly evident and you note in the discussion around line 465 that this could be related to the use of the red band. So I don't understand why you do not explore using the Green band on its own, or like the L8 method, in cooperation with the Red Band?

*Thanks for the suggestion. We had previously conducted the analysis for the green band but chose to exclude it from the manuscript because the depths that were produced for Sentinel-2 were much too high relative to those calculated for Landsat 8: for example, maximum predicted lake depths from Sentinel-2 were ~19 m, compared with values of only ~5.5 m in the Landsat 8 data. However, we have now decided to include this analysis in the paper as a supplementary figure (and with details of the derived relationship in text and in Table 1), in a similar way to the empirical relationships as applied to the green-band and blue-band data, as we think that it will be helpful for other workers in the future. Given that there was such over-prediction by the green band, we chose not to conduct any joint analysis involving using both the green and red bands. We do think that future work would be merited, however, to help overcome the issue of saturation in the Sentinel-2 red band technique, but we are aware that this is an issue that also exists for Landsat 8, as documented in previous work.*

In addition, Figures 3 and 4 (and other similar) would benefit from using heat maps rather than small dots; the data density is too high for interpretation in this format. Using a 1:1 line (or similar) might also help in interpretation.

*Thank you for the suggestion, but we think that a heat map format would not work well here, because we are trying to display two sets of data on a single figure, and as it stands, the data points are displayed in a semi-transparent way to show the locations on the plot where there are more data points. This means it is possible to see where the data overlap from different dates, while ensuring that all of the data are still visible. Thus, we think that the figure formats we have chosen work in a similar way to a heat map but also allow two sets of data to be displayed at once. However, we have added a 1:1 line to aid with interpretation, as requested, as we think that this is very helpful.*

## Analysis: Error & How Many Lakes?

This study would be more robust if a little more attention was added to areas that help contextualize the data. In particular:

- Adding any error bars on values which are calculated for area / volume

*Apologies, we overlooked including them. Added.*

- For volume (e.g. Line 334), a 10% disagreement between S2 and L8 seems pretty good. However, a big factor that has the potential to be quite variable between image resolutions, is the calculation of the lake shore and therefore lake bottom albedo. Did you explore this effect at all? Or at least it might be good to include it in the discussion?

*This was something we did briefly explore in the earlier analysis (for scene-by-scene lake-depth calculations), and the result for Sentinel-2 was including a lake shore comprising the lake-area mask dilated by two pixels (i.e. 20 m) instead of a single pixel (i.e. 10 m). We have now included an extra clause here to explain that it is crucial to ensure that the lake-bottom albedo values are correctly defined given the sensitivity of the method to this parameter, and this is why we chose to include two pixels around the lake edge.*

- In Line 330, you observe more lakes in the dual record than in L8 or S2 individually. Why isn't there more match-up of the lakes being tracked in the individual datasets? Is this a result of the higher temporal density? Cloud cover differences? Other? I'm curious because the tests in the Supplement seem to show such close agreement in lake areas being measured.

*The comparisons of lake area presented in the Supplement were only for lakes that were present in both the Landsat 8 and Sentinel-2 datasets, which explains the close agreement between the two sets of values. The reason that more lakes are present in the dual-satellite record than either record individually is because of the dual-satellite record's higher temporal resolution. This results in a greater number of pixels across the whole image stack being marked as water-covered using the dual-satellite record at least once in the season, and thus being included in the calculations of maximum lake extents across the whole season. When we then filter out groups of pixels that do not reach more than 495 pixels at least once in the season (see Sect. 2.5.1), more groups of pixels meet this size with the dual-satellite record than with either record individually, and so more lakes are tracked. We hope that this makes sense.*

## The Role of Opened Conduits:

There is an assumption that one lakes drain quickly (by opening a conduit) that these conduits continue to remain open. However, there is no discussion about whether this assumption is theoretically sound or observationally verified. Is this equally likely for small and large lakes at various ice sheet thicknesses / stress states? There seem to be a lot of variables, and this may indeed be valid, but it should be explained – in particular given the conclusions related to the role of small lakes connecting the supraglacial and subglacial hydrological systems.

*We agree that this is indeed an assumption with this method. We have now chosen to acknowledge that there is an assumption that the moulins will remain open more clearly at several places in the manuscript, including in the discussion, where we have stated that this assumption may vary across the study region according to ice thickness or stress state, for example.*

Other minor comments:

Line 8: Landsat is still what I would call medium resolution, especially with a new era of sub-metre sensors. Maybe fix by changing “high spatial resolution” to “higher spatial resolution”?

*Done.*

Line 131: Have you considered providing tables in txt form, too (or perhaps provided with code to batch download) to facilitate reproducibility?

*Full source code for the FASTER algorithm is now available online publicly to facilitate reproducibility; please also see response to the later comment on the same topic of distributing data.*

Line 141: You write that tiles were reprojected. How were data interpolated – NN, bilinear, other? These details were carefully described in other steps, so I ask mostly for completeness.

*Thanks for noting the omission. This was bilinear interpolation – now clarified in text.*

Line 148: For those less familiar, perhaps write “band-6” as “SWIR/band-6” or similar? Here and elsewhere.

*Done here and elsewhere.*

Line 151: For cloud shadow – I don’t know that this is enough to handle shadow. Did you check any math / assumptions (based on cloud elevation, solar angle, etc.) that this would really be sufficient? It could be a big deal, especially for false-positives on fake drainage. Again, I’m really unsure and haven’t run the numbers myself, but it seems important enough to confirm.

*That was unclear, apologies. Images were manually verified for shadowing. This has been clarified in text. The 200 m value was chosen based on manually inspecting images with the thresholds applied, and occasionally some finer clouds near to the edges of larger clouds had been missed with the classification, and a 200 m radius helped to remove them. An alternative automated approach would be to include a filter based on the temporal consistency (see Williamson et al., 2017 for an example) to separate lakes (which are more persistent) from shadows (which are less persistent), but we did not see that shadowing was a large issue in this study, so we chose not to do this.*

Line 154: For lack of a better place to put this: I believe that L8 and S2 are orthorectified using different DEMs, so there could be (slight) offsets in lake locations. Have you considered this effect or the magnitude in it? The Kaab/Paul 2016 papers you referencing think about implications for velocity tracking, but I’m just not sure of the impact in this part of the world.

*True – we have now mentioned this in the manuscript. We manually checked for lake offset on two contemporaneous image pairs (1 July and 31 July 2016), but did not note any obvious offset.*

Line 159: You use the cloud masks provided with the data, but is there any evidence on reliability over snow and ice?

*This step was only an initial means to filter images that were likely to be particularly cloudy. Before an image was excluded entirely, it was manually checked, to ensure that the cloud mask provided with the data had produced a reliable measure of cloudiness. The actual cloud-masking steps were different (as described later in that section).*

Figure 2: Reprojecting step not included?

*We think that this is quite difficult to include on the figure without making it more confusing, but we have now explained in the figure caption that the steps referenced apply once the reprojection has been completed. Hopefully this is satisfactory.*

Figure 2: I believe lake area masks should feed into lake depth calculation (e.g. finding lake edges)?

*That's correct, thanks for highlighting the issue. Now corrected.*

Line 180: The resampling and NDWI steps appear to be described in Figure 2 in the opposite order?

*That was incorrect in text and correct on Figure 2. We've altered the text.*

Line 231: Not an issue – I'm mostly just curious – why you chose NN here (and bilinear elsewhere)?

*This was to avoid any smoothing of the values associated with bilinear interpolation, which we think would introduce errors into the depth and thus volume calculations.*

Line 241: Well done with these acronyms

*Thank you!*

Figure 3 & 4: Include legend so figure is easier to read

*Done.*

Line 336: Are these symmetrical distributions? Perhaps using Quartile1 / Quartile3 info will help describe the data while also being sure to use non-parametric statistics.

*This information has been added alongside a correction to the values presented in the original manuscript (which stemmed from including values of 0 in the original analysis).*

Line 341: Did you ever compare with MODIS to make that the \*it\* failed the test (as it would be expected to)?

*Unfortunately, we didn't do any direct MODIS comparisons in this study because we didn't have the 2016 MODIS imagery downloaded and processed (and we think the paper is already sufficiently detailed without any such comparisons), but it is certainly something that could be done in future work.*

Figure 6/7: I really like how you can display the data in the context of which data is available!! Have you considered if there was any variability in lake distribution / more nuanced than just scaling by cloud cover percent? Like an elevation-dependent extrapolation, or something like that? Also: consider combining into one figure

*Thanks for the suggestion to scale the lake data in other ways. We didn't do anything of this sort in this study, but it would certainly be possible to do, even though it would of course have an associated caveat that it would not necessarily result in an accurate representation of the data (as indeed is also true when scaling by cloud cover and regional data cover). To address the second part of the comment, we think it is preferable to keep these as two separate figures as they show two different sets of data that may otherwise be confusing, so have not combined them into a single figure.*

Figures 8 & 9: Combine into one figure

*Again, we think that these are better as two separate figures as they display different things altogether, so have not made this change.*

Fig 11: These colors are not necessarily all distinguishable to a color-blind reader. Revise colors and/or label the lines on the righthand axis.

*Thanks for pointing that out. We have labelled the lines on the right-hand axis as per your suggestion.*

Line 578: What about sharing your resultant lake dataset? Line 578: The Cryosphere data policy encourages a few things that are different from how this paper handles sharing – most importantly share data AND code in an open, citable repository. Requiring to ask an author is a large barrier particularly in the future. See Gil et al. for further suggestions, and I'm sure that your readership would love to have these tools and dataset available in an open place / GitHub repo.

<https://agupubs.onlinelibrary.wiley.com/doi/full/10.1002/2015EA000136>

*Thank you for this suggestion – we had overlooked the specific data policy of The Cryosphere. The full FASTER source code is now available publicly (and is appropriately referenced within the manuscript) with an embargo for a year to allow other pieces of ongoing work using this code to be completed. However, individuals are able to request the code via the link provided, and their requests will be approved by me. After the embargo expires, the full code will be available to anyone. Access to the source code allows other workers to reproduce the outputs of this work.*

## Response to reviewer #2 (Samuel Doyle)

Williamson et al. present a new technique which combines two different types of satellite imagery to create a lake geometry time series with an unprecedented combination of spatial and temporal resolution. The methods are rigorous and described in comprehensive detail. Indeed the detailed description of the methods gives the impression that the manuscript is largely a techniques paper despite significant results also being presented. The figures and tables are of a high standard and the referencing is appropriate throughout. The manuscript reads well with very few errors. The finding that a large proportion of surface water drains through small (and often previously undetected) lakes is significant. The paper builds on previous work on supraglacial lakes on the Greenland ice sheet.

*We are very appreciative of the positive remarks, thank you.*

### General comments

My main concern stems from L213: “*We treated these Landsat depths and volumes as ground-truth data as in Williamson et al. (2018)*”. This assumption is not discussed in detail at any point in the manuscript, although I guess it may have been described in the author’s previous paper. In my opinion, there should be more discussion in this manuscript of the lack of actual ground truthing and how this might affect the absolute accuracy of the results. That is, how do the authors expect the results to compare with reality? How does this study compare to previous studies which employed ground truthing? To be clear, I’m not expecting ground truthing to be undertaken, but the lack of ground truthing and its potential effects should be discussed.

*This was indeed discussed in one of my previous papers; however, we have now added an additional paragraph at the end of discussion Sect. 4.1 to include further justification for using the Landsat 8 data as ground-truth data, and the limitations that are inherent in their use as such. We also mention how future work may take this initial work forward, which would include comparing the Sentinel-2 lake-depth measurements with ‘better’ or other ground-truth data, such as higher-resolution satellite-imagery measurements or field data of lake depth. We hope that this addresses your concern sufficiently.*

There is also a lack of discussion of the depth limitation of the techniques used. The techniques presented only retrieve lake depth up until a certain point. Figures 3 and 4 suggest a 6 m limit, when lakes are known to be often deeper than 10 m. If many lakes are deeper than the limit then this would hypothetically create a bias in the results by underestimating the volumes of the deeper lakes, which could affect the reliability of the main conclusion of the paper — that the water drained through small lakes is greater than that through large lakes. Given this, the relatively low maximum lake volumes ( $1.2 \times 10^7 \text{ m}^3$ ) reported on L334/335 compared to those in the literature (e.g. Box and Ski, 2007) are potentially concerning. These limitations should be discussed to make the reader aware of them. The authors could also look to previous studies, which have measured lake depths to understand whether the maximum depth of their technique is potentially too shallow.

*Thanks for pointing this out. We agree that the depth and volume measurements are lower than those that have been observed in the field and this is likely to be due to the sensitivity of the physically based methods for measuring lake depth (i.e. the red wavelengths become fully attenuated in the water column). This effect is present for all remote-sensing imagery as far as we are aware, with previous studies showing the same for WorldView-2 (Moussavi et al., 2016), Landsat 8 (Pope et al., 2016) and MODIS*

*(Williamson et al., 2017). The same problem would not necessarily exist with empirical techniques for calculating lake depth remotely, e.g. a method to scale reflectance to depth based on field measurements of depth (e.g. Fitzpatrick et al., 2014); however, they require field data, and site- and time-specific tuning and are not physically based. We think that the limitations of the physically based technique for calculating lake depth are already sufficiently discussed in Sect. 4.1. But, we have now included an extra clause where we explain that the effect of these limitations may be an under-measurement of lake volume compared with previous work (e.g. Box and Ski, 2007). However, it should be noted that, while the maximum volumes are larger in their study, the lake volumes calculated using our technique are of the same order of magnitude as many of the other values presented in their study (e.g. their Table 5). We also think that the conclusions relating to the water drained after small lakes have opened-up moulins are independent of the method for calculating lake depth and volume (since they are based on the identification of lake drainage and the runoff data derived from a different data product), so overall do not think that this creates concern over the reliability of this conclusion.*

These issues aside, the discussion of problems and limitations in Section 4.1 is well- considered and appropriate.

*Thank you.*

### **Specific comments**

L24/25 — consider offering an explanation for why small lakes drain such a large proportion of the runoff. Is it because they are more numerous? An explanation for this observation is never given in the manuscript.

*Clarified that this is indeed a product of the more numerous small lake-drainage events that allow more moulins to open and the fact that small lakes are usually at lower elevations.*

L29 — the last two references in this sentence are in the wrong place. They currently only relate to there being two main ways the ice sheet loses mass (without specifying what they are), which as a statement does not need a citation. Perhaps move them to later in the sentence/paragraph.

*Moved to later in the paragraph.*

L40 — I'm not sure whether the citations to Doyle et al. (2018) and Hofstede et al. (2018) are appropriate here. Presumably they are given here as evidence for subglacial sediment? In fact the number of citations given here could be significantly reduced to list only the key studies.

*Apologies, the referencing here was unclear: some of the references related to observations of enhanced sliding over hours to day associated with surface melt delivery to the bed, and some of the references related to the potential for increased flow speeds when meltwater reaches the bed if the Greenland Ice Sheet is underlain by sediment. This is now hopefully clearer in the revised manuscript.*

L43 — Consider the recent paper by Christoffersen et al. (2018) here.

*Included.*

L44 — It is well established that surface water delivered to the bed of the Greenland ice sheet accelerates ice flow in the short term. Given the evidence for this, the phrase ‘potentially explaining’ seems a bit weak.

*Removed ‘potentially’.*

L45 — Consider citing Joughin et al. (2013) and Hoffmann et al. (2011) here.

*Added.*

L75 — I’m not aware of any evidence which suggests lake hydrofracture takes days. All the evidence suggests the process is rapid, taking hours or less.

*Changed.*

L111 — May to October is not summer, perhaps use ‘melt season’ instead, although there is not usually much melt in October.

*Changed.*

L124 — Why does the study only cover up to 90 km inland? Perhaps give a reason here.

*Clarified in text. It’s related to the size of the original Sentinel-2 tiles.*

L187 — stating the increments provides no information on how much it was adjusted in absolute terms, unless only one increment was used? Or is the percentage change given per 0.01 increment? Please clarify.

*Clarified in text.*

L230 — Can you (briefly) be a bit more specific here as to how the new technique was validated, even if it requires some repetition.

*This information is included at the end of this paragraph in the sentence beginning: “To evaluate the performance ...” We have now also added an extra clause here to remind the reader of the validation procedure.*

L260 — Consider discussing the implications of Cooley and Christoffersen (2017) regarding the effects of observation bias on the detection of rapidly draining lakes. The reduced interval of the new technique presented in the manuscript under review should reduce the observation bias associated with the longer intervals of previous studies.

*Thanks for that suggestion. We think that this comment fits better towards the end of discussion Sect. 4.3, so have added it there.*

L271 and L418 and L496 and elsewhere — The term ‘interior’ is here used as a synonym for ‘englacial’. This is arguably ambiguous with the frequent use of ‘interior’ to describe the central region of the ice sheet (including the surface) away from the margin. The use of this term here also neglects the important effects of surface water reaching the bed.

*Altered to 'internal hydrological system' here and throughout.*

L335 — These maximum volumes seem quite low. How do they compare with the literature? Are there any reasons why the volumes are low? Is it due to the depth limitation of the techniques used?

*This has now been discussed in Sect. 4.1. And please also see the response to the earlier comment relating to this.*

L411 — The two modelling studies cited here were not the first to suggest this. Consider citing other studies and/or adding an e.g. before the citation.

*Added 'e.g.' before.*

L418 — Why is this? Why does more water drain through small lakes than larger ones? Can it be explained by the greater number of small lakes, or is it a result of drainage basin size, or is it a result of a bias in the technique? Some discussion is warranted.

*This has now been clarified in the text (discussion Sect. 4.3) to be a result of the greater number of small lakes and the fact that they are found at lower elevations than large lakes, where melting is higher.*

L503 and other occurrences of this pair of citations — these modelling studies may not be considered as the first or most appropriate for the establishment of drainage through moulins, which has been known for a long time (and was not determined by modelling). Consider listing earlier citations and/or giving an e.g. first to show that these citations are selected examples. Some of the sentences preceding these citations (including that on L503) may not even need a citation.

*This has been clarified with an "e.g." has been added. We think that the citations in the previous line are required, so have not made a change.*

L511 — 'runoff' not 'meltwater'.

*Changed.*

L512 — 'the moulins'.

*Changed.*

Fig. 1 — Consider labelling some glaciers to aid the reader. Also, consider showing enlarged images of each of the two example lakes as subplots to demonstrate the capability and resolution of the imagery.

*Glaciers now labelled, thank you for suggesting. Enlarged image shown of the rapidly draining lake in the green box.*

Fig. 3 — at this scale, whether the markers are circles or squares is redundant.

*Changed reference to 'circles' and 'squares' to 'markers' where relevant, and now included a legend on the figure (as per reviewer #1's suggestion) to show this information.*

Fig. 10 — consider a red/blue transparency with purple overlap (or any other primary colour pair).

*Changed.*

### **Technical corrections**

L20 — ‘identify’ is the wrong word here, suggest ‘estimate’

*Changed.*

L25 — strictly speaking its not via *all* moulins but only those identified within ‘small’ and ‘large’ lakes.

*Changed.*

L95 — define MSI.

*Done.*

L112 — the last sentence of this aim isn’t written as an aim and there is change of tense from the adjacent sentences.

*Changed.*

L114 — define ‘rapidly’ here.

*Done.*

L208 and other occurrences — within the text write out ‘Section’ or ‘Figure’ in full.

*This is contradictory to the journal’s house standards (where Sect. and Fig. are used in running text, unless at the start of a sentence), so this change has not been made.*

L258 — citation should be to Doyle et al. (2013).

*Changed.*

L297 — replace ‘more poorly’ with ‘worse’.

*Changed.*

L330 — what does the number in brackets refer to?

*Clarified.*

L376 — Suggest: ‘when the pair of images were only separated by a day’.

*Changed.*

L391 — “Large lakes are *defined as . . .*”

*Changed.*

L396 and L405 and L428 — Write out ‘Figure’ within text.

*This is contradictory to the journal’s house standards (where Sect. and Fig. are used in running text, unless at the start of a sentence), so this change has not been made.*

L434 — consider rearranging to avoid double brackets.

*Done.*

L465 — ‘entirely’ is not necessary here.

*Removed.*

L490 — ‘offset’ is the wrong word here.

*Changed.*

Table 2 — Consistency with precision. Specifically, minimum drainage volume should be given as 0.020 for large lakes for Sentinel 2 (not 0.02). The same applies to the same for Landsat 8.

*Changed.*

Section S1 — delete ‘the value of’ in the first sentence.

*Done.*

Table S2 — Write out ‘The asterisk denotes . . . ’

*Done.*

Fig. S1 — Overlap in X-axis label superscript. Also, consider inserting ‘therefore’ in ‘. . . between the two sets of lake areas is *therefore* remarkably small’.

*Changed.*

#### **Additional references (not already cited in the manuscript)**

Christoffersen, P., Bougamont, M., Hubbard, A., Doyle, S.H., Grigsby, S. & Pettersson, P. 2018. Cascading lake drainage on the Greenland ice sheet triggered by tensile shock and fracture, *Nature Comms.*, 9 1064.

Cooley, S. W., & Christoffersen, P. (2017). Observation bias correction reveals more rapidly draining lakes on the Greenland Ice Sheet. *Journal of Geophysical Research: Earth Surface*, 122, 1867—1881

Joughin, I., Das, S., Flowers, G., Behn, M., Alley, R., King, M., Smith, B., Bamber, J., van den Broeke, M. & van Angelen, J. 2013. Influence of ice-sheet geometry and supraglacial lakes on seasonal ice-flow variability, *The Cryosphere*, 7, 1185-1192.

## Response to reviewer #3 (Kristin Poinar)

### Summary

Williamson et al describe a substantial new contribution to the remote-sensing detection of Greenland supraglacial lake drainage events. Their approach is to combine images from two medium- to high-resolution sensors to achieve near-daily time resolution of a study area in WNW Greenland. The authors apply this new technique over the 2016 melt season and are able to detect smaller draining lakes ( $<0.125 \text{ km}^2$ ) than previously possible, with good temporal precision ( $\pm \sim 1$  day). By combining the new lake drainage dataset with regional climate model output analyzed across surface catchments, the authors conclude that smaller ( $<0.125 \text{ km}^2$ ) fast-draining lakes, which previous coarser analyses have missed, actually contribute a majority of lake water to the subglacial system across the study area. Their result shows the importance of using high-res techniques, such as presented here, to identify the locations and timing of lake water input to the subglacial system.

*Thank you for the positive comments.*

### Specific comments

The methods portion of the paper is thorough and appears to be robust; the study uses previous work (by Pope and by Williamson) to validate its new methods.

In the results portion, it was unclear which data were used to develop the empirical relationships between L8 lake depth and S2 TOA reflectance (July 1 / 31?), and which data were used to evaluate it (Table 1; all image dates?). Perhaps the distinction is not of great importance (I cannot tell), but this could be easily clarified.

*Apologies that this was unclear. We have now clarified it in Sect. 3.1.*

I would suggest against the use of the word “error” in lake-drainage dates. “Error” suggests that the true dates of lake drainage are known; however, they are not known. “Precision” would thus be a more accurate term.

*Changed throughout, thank you for the suggestion.*

Given the new ability to precisely identify drainage dates of more lakes than ever before, I read the Discussion with great interest. I think two of the inferences made in this section were a bit weak. However, these were not the main contribution of the work, and so scaling them back will not make a great loss to the paper.

1. Lake size and lake drainage date – The authors attribute the high water contribution (61.5%) by small lakes to the fact that they drain earlier in the melt season than large lakes (lines 511-512). While the data in Table 2 do show a significant difference (non-overlapping date ranges) between small and large lake drainage dates, this difference (just 1-2 days) is not substantial within the context of the melt season and the evolution of subglacial hydrology.

*Yes, this is true, and so we have now played this down, thank you for pointing it out. The high water contribution by moulins from small lakes is due to the difference in elevation of the two lake types and the fact that small lakes are more numerous.*

2. Lake size and elevation – The authors also state that the lower elevations of small lakes may contribute to their greater water contribution (lines 512-513). These data do not appear in Table 2 (I would suggest adding it: the mean and std elevations of large and small lakes), and this statement contradicts another statement (lines 400-402) that lake size and elevation are uncorrelated.

*There is a difference in the mean elevations of the small versus large lakes (small lake mean elevation = 697 m a.s.l.; large lake mean elevation = 848 m a.s.l.), which likely explains some of the difference in their water contribution. The statement at lines 400-402 was poorly expressed, meaning to indicate that the two lake types might appear to be randomly distributed across the region; however, a closer examination does appear to suggest that there are more smaller lakes at lower elevations in the north of the region. This has been amended in the manuscript.*

What, then, can explain the high (61.5%) contribution of the small lakes? Is it simply a large total size of their basins? This information would be easy to include (I believe it is already calculated).

*This has now been clarified to be a result of both the lower elevation of small lakes compared with large ones, and the fact that there are more small lakes. In text, the mean and standard deviations of small lakes have been added (Sect. 4.3) to demonstrate this point. In addition, the slight difference in drainage dates likely has some effect, but we agree that this is likely to be only minimal, so we have not removed it entirely, but toned it down.*

Finally, and most crucially, the conclusion that small lakes are important to the subglacial hydrological system is based on the assumption that their moulins stay open for the entire melt season (Figure 11). I don't have any especial reason to doubt this, but the assumption is not backed up in the paper although I believe the authors' data could easily do so. Presumably, if a moulin were to close up before the end of the melt season, a lake would re-form on site, and could be seen in the data. I think I can infer from the description of the FASTER algorithm that any such lakes would not meet the criteria for "fast-draining" and thus would not be included in this study – but this is not stated/explained in the manuscript.

*We have now acknowledged the assumption that the moulins must remain open more clearly at several places in the manuscript, and in the discussion have stated that this may vary across the study region according to ice thickness or stress state, for example. The FASTER algorithm would filter out some lakes in the way you suggest since it filters lakes that re-fill on the subsequent day of cloud-free imagery by more than 20% of the total water volume lost during the drainage event. So, these lakes would not be included in the analysis. However, lakes that refill later in the season are not excluded from the "fast-draining" category in the way suggested above, so it is difficult to verify the assumption using the data available to us. In addition, testing this assumption using the FASTER algorithm in the way suggested assumes that there is sufficient melt to fill a basin after it has drained and the moulin has closed up. We think that acknowledging the assumptions inherent in our method is sufficient to justify the conclusion relating to the importance of small lakes.*

## **Technical comments**

Line 7 - I wouldn't start the abstract with "Although"; move it to the middle of the sentence as "however".

*Changed.*

Lines 47, 49 - It is not sensible heat, but latent heat that makes both of these effects (Phillips and Mankoff references). Water temperature is not important.

*Removed references to temperature.*

Line 49 - It's actually Poinar et al. 2016 (not 2017)

*Apologies, but we think that our original reference was correct. We believe that the final publication date of the article in question was 2017, even though it was initially accepted and appeared online on the Journal of Glaciology website under FirstView in 2016. <https://doi.org/10.1017/jog.2016.103> for details.*

Line 67 - Replace "this" with its antecedent (since it is the first sentence of the paragraph).

*Done.*

Line 82 - The records have no problems; instead, perhaps the methods have shortcomings.

*Altered.*

Lines 85 and 95 - Define or remove SAR, MSI acronyms

*Both defined.*

Line 135 - Clarify year 2016

*Done.*

Lines 155, 159 - I got a bit confused with the numbers here, since they are similar ( $38 + 39 = 77$ ). Perhaps recast the sentences to use only the number 39. Also please state the year 2016 again here.

*Done.*

Line 190 -  $R^2 = 0.999$ , that's excellent, good for you!

*Thank you!*

Line 271 and elsewhere - "GrIS interior" confused me; to me it means inland or upstream regions, whereas you intend to say that the water leaves the surface and enters the englacial or subglacial environment.

*Clarified as 'internal hydrological system' throughout.*

Line 294 - Here you say ~3 meters but later (line 465) you say ~3.5 meters.

*Changed to 3.5 metres in both instances.*

Lines 347-350 - This sentence would benefit from parallel construction.

*Changed to add a colon to link the sentences to show that the second clause logically follows from the first.*

Line 353 -  $p=0.00$  should be more precise.

*Clarified, although the value we have now included is essentially meaningless as it is so small!*

Line 443 - “We opted for” sounds a bit informal.

*Changed.*

Lines 458-468 - Effect of July 1 “cloud adjacency”. Pixels 200 m from clouds were already removed (Data and methods section), so it seems to me that this cloud-adjacency argument would not apply. Perhaps more description of how “adjacent” (i.e., if there are effects >200 m away) these effects are is required.

*This has been clarified that there may have been effects at > 200 m distance from the clouds.*

Lines 536-539 - It reads a little harsh on Miles et al. to end the paragraph with the shortcomings of that study; instead wouldn't it be better to end by highlighting the strengths of your own study?

*This paragraph has been restructured and reworded to deal with this comment.*

Lines 540-541 - As written, this sentence is false because other studies have combined two optical satellite datasets (e.g. MODIS and L8). Recast by adding “medium- resolution” or moving the sensors out of parentheses.

*Changed.*

Line 561 - “less” instead of “not”

*Changed.*

Figure 7. I like that Figure 6 was scaled up to the full image region here. The data show a lot of variability (sawtooth-like) on multi-day scales. I'd be interested in whether this is “real” (perhaps regionally linked lake drainages?) or just noise remaining from the effects of clouded-over regions.

*This is essentially noise in the data. It likely stems from the fact that even if there is lower regional cover on a single day (e.g. large areas of cloud or no-data values), and the data are scaled accordingly with these values, this method does not take account of precisely where the missing data are relative to the locations of actual observations on the image. Of course, it is indeed likely that some of the changes are indeed volume loss from the surface due to lake drainage, but these are not separated out here. So, Figure 7 really just presents an estimate of how the data might look, with some of the patterns being unrealistic.*

Figure 10. The magnitude of lake volume (x axis) seems much too large: the largest lake would have a volume of  $10^{16} \text{ m}^3$ , which would be 100 km x 100 km x 10 km, way too big. There must be an error here.

*Apologies, this was an incorrectly labelled x-axis; these values were calculated by taking the natural logarithm of the original values, not the logarithm to the base 10. The label has been updated.*

Figure 11. The y axis label is confusing: volume, yet mm?

*This was incorrect, we apologise, and was only something we became aware of after the manuscript had entered review. We have now included an updated figure.*

Table 2. Consider adding the mean surface elevation of the 3 classes of lakes, as described in the “Specific comments” section of this review.

*The mean and standard deviation of the small and large lakes are now clarified in text.*

# Dual-satellite (Sentinel-2 and Landsat 8) remote sensing of supraglacial lakes in Greenland

Andrew G. Williamson<sup>1</sup>, Alison F. Banwell<sup>1,2</sup>, Ian C. Willis<sup>1,2</sup>, Neil S. Arnold<sup>1</sup>

5 <sup>1</sup>Scott Polar Research Institute, University of Cambridge, Cambridge, UK

[<sup>2</sup>Cooperative Institute for Research in Environmental Sciences, University of Colorado Boulder, Boulder, Colorado, USA](#)

Correspondence to: Andrew G. Williamson (agw41@[alumni.cam.ac.uk](mailto:alumni.cam.ac.uk))

**Abstract.** ~~Although R~~ Remote sensing is commonly used to monitor supraglacial lakes on the Greenland Ice Sheet; ~~however,~~ most satellite records must trade-off higher spatial resolution for higher temporal resolution (e.g. MODIS) or vice versa (e.g. Landsat). Here, we overcome this issue by developing and applying a dual-sensor method that can monitor changes to lake areas and volumes at high spatial resolution (10–30 m) with a frequent revisit time (~3 days). We achieve this by mosaicking imagery from the Landsat 8 OLI with imagery from the recently launched Sentinel-2 MSI for a ~12,000 km<sup>2</sup> area of West Greenland in summer 2016. First, we validate a physically based method for calculating lake depths with Sentinel-2 by comparing measurements against those derived from the available contemporaneous Landsat 8 imagery; we find close correspondence between the two sets of values ( $R^2 = 0.841$ ; RMSE = 0.555 m). This provides us with the methodological basis for automatically calculating lake areas, depths and volumes from all available Landsat 8 and Sentinel-2 images. These automatic methods are incorporated into an algorithm for Fully Automated Supraglacial lake Tracking at Enhanced Resolution (FASTER). The FASTER algorithm produces time series showing lake evolution during the 2016 melt season, including automated rapid ( $\leq 4$  day) lake-drainage identification. With the dual Sentinel-2–Landsat 8 record, we identify 184 rapidly draining lakes, many more than identified with either imagery collection alone (93 with Sentinel-2; 66 with Landsat 8), due to their inferior temporal resolution, or would be possible with MODIS, due to its omission of small lakes  $< 0.125$  km<sup>2</sup>. Finally, we ~~identify-estimate~~ the water volumes drained into the GrIS ~~during~~ rapid lake-drainage events and, by ~~using~~ analysing downscaled regional climate-model (RACMO2.3p2) runoff data, the water quantity that enters the GrIS via the moulins opened by such events. We find that during the lake-drainage events alone, the water drained by small lakes ( $< 0.125$  km<sup>2</sup>) is only 5.1% of the total water volume drained by all lakes. However, considering the total water volume entering the GrIS after lake drainage, the moulins opened by small lakes deliver 61.5% of the total water volume delivered via ~~all the~~ moulins ~~(i.e. opened by large and small lakes)~~; this is because there are more small lakes, allowing more moulins to open, and because small lakes are found at lower elevations than large lakes, where runoff is higher. These findings suggest that small lakes should be included in future remote sensing and modelling work.

## 30 1 Introduction

In the summer, supraglacial lakes (hereafter “lakes”) form within the ablation zone of the Greenland Ice Sheet (GrIS), influencing the GrIS’s accelerating mass loss (van den Broeke *et al.*, 2016) in two main ways ~~(Chu, 2014; Nienow *et al.*, 2017)~~. First, because the lakes have low albedo, they can directly affect the surface mass balance through enhancing ablation relative to the surrounding bare ice (Lüthje *et al.*, 2006; Tedesco *et al.*, 2012). Second, many lakes affect the dynamic component of the GrIS’s mass balance when they drain either “slowly” or “rapidly” in the mid- to late melt season (e.g. Palmer

*et al.*, 2011; Joughin *et al.*, 2013; [Chu, 2014](#); [Nienow \*et al.\*, 2017](#)). Slowly draining lakes typically overtop and incise supraglacial streams in days to weeks (Hoffman *et al.*, 2011; Tedesco *et al.*, 2013), while rapidly draining lakes drain by hydrofracture in hours to days (Das *et al.*, 2008; Doyle *et al.*, 2013; Tedesco *et al.*, 2013; Stevens *et al.*, 2015).

Rapid lake drainage plays an important role in the GrIS's negative mass balance because the large volumes of lake water can reach the subglacial drainage system, perturbing it from a steady state, lowering subglacial effective pressure, and enhancing basal sliding over hours to days ([Shepherd \*et al.\*, 2009](#); [Schoof, 2010](#); [Bartholomew \*et al.\*, 2011a, 2011b, 2012](#); [Hoffman \*et al.\*, 2011](#); [Banwell \*et al.\*, 2013, 2016](#); [Tedesco \*et al.\*, 2013](#); [Andrews \*et al.\*, 2014](#)), particularly if the GrIS is underlain by sediment ([Shepherd \*et al.\*, 2009](#); [Schoof, 2010](#); [Bartholomew \*et al.\*, 2011a, 2011b, 2012](#); [Hoffman \*et al.\*, 2011](#); [Banwell \*et al.\*, 2013, 2016](#); [Tedesco \*et al.\*, 2013](#); [Andrews \*et al.\*, 2014](#)); [Bougamont \*et al.\*, 2014](#); [Kulesa \*et al.\*, 2017](#); [Doyle \*et al.\*, 2018](#); [Hofstede \*et al.\*, 2018](#); ~~[Koziol and Arnold, 2018](#)~~). Rapid lake-drainage events also have two longer-term effects. First, they open moulins, either directly within lake basins (Das *et al.*, 2008; Tedesco *et al.*, 2013) or in the far field if perturbations in stress exceed the tensile strength of ice (Hoffman *et al.*, 2018), [sometimes leading to a cascading lake-drainage process](#) ([Christoffersen \*et al.\*, 2018](#)). These moulins deliver the bulk of surface meltwater to the ice-sheet bed (Koziol *et al.*, 2017), ~~potentially~~ explaining the observations of increased ice velocities over monthly to seasonal timescales within some sectors of the GrIS (Zwally *et al.*, 2002; Joughin *et al.*, 2008, [2013](#), 2016; [Bartholomew \*et al.\*, 2010](#); [Colgan \*et al.\*, 2011](#); [Hoffman \*et al.\*, 2011](#); [Palmer \*et al.\*, 2011](#); [Banwell \*et al.\*, 2013, 2016](#); [Cowton \*et al.\*, 2013](#); [Sole \*et al.\*, 2013](#); [Tedstone \*et al.\*, 2014](#); [Koziol and Arnold, 2018](#)). Second, the fractures generated during drainage allow ~~warmer (> 0 °C)~~ surface meltwater to reach the subfreezing ice underneath, potentially increasing the ice-deformation rate over longer timescales (Phillips *et al.*, 2010, 2013; Lüthi *et al.*, 2015), although the magnitude of this effect is unclear (Poinar *et al.*, 2017). Alternatively, the ~~warmer~~ water might promote enhanced subglacial conduit formation due to increased viscous heat dissipation (Mankoff and Tulaczyk, 2017). Although rapidly and slowly draining lakes are distinct, they can influence each other synoptically if, for example, the water within a stream overflowing from a slowly draining lake reaches the ice-sheet bed, thus causing basal uplift or sliding, and thereby increasing the propensity for rapid lake drainage nearby (Tedesco *et al.*, 2013; Stevens *et al.*, 2015).

While lake drainage is known to affect ice dynamics over short (hourly to weekly) timescales, greater uncertainty surrounds its longer-term (seasonal to decadal) dynamic impacts (Nienow *et al.*, 2017). This is because the subglacial drainage system in land-terminating regions may evolve to higher hydraulic efficiency, or water may leak into poorly connected regions of the bed, producing subsequent ice-velocity slowdowns either in the late summer, winter or longer term (van de Wal *et al.*, 2008, 2015; [Bartholomew \*et al.\*, 2010](#); [Hoffman \*et al.\*, 2011, 2016](#); [Sundal \*et al.\*, 2011](#); [Sole \*et al.\*, 2013](#); [Tedstone \*et al.\*, 2015](#); [de Fleurian \*et al.\*, 2016](#); [Stevens \*et al.\*, 2016](#)). Despite this observed slowdown for some of the GrIS's ice-marginal regions, greater uncertainty surrounds the impact of lake drainage on ice dynamics within interior regions of the ice sheet, since fieldwork and modelling suggest that increased summer velocities may not be offset by later ice-velocity decreases (Doyle *et al.*, 2014; [de Fleurian \*et al.\*, 2016](#)), and it is unclear whether hydrofracture can occur within these regions, due to the thicker ice and limited crevassing ([Dow \*et al.\*, 2014](#); [Poinar \*et al.\*, 2015](#)). [These unknowns inland](#) add to the uncertainty in predicting future mass loss from the GrIS. There is a need, therefore, to study the seasonal filling and drainage of lakes on the GrIS, and to understand its spatial distribution and inter-annual variation, in order to inform the boundary conditions for GrIS hydrology and ice-dynamic models ([Banwell \*et al.\*, 2012, 2016](#); [Leeson \*et al.\*, 2012](#); [Arnold \*et al.\*, 2014](#); [Koziol \*et al.\*, 2017](#)).

Remote sensing has helped to fulfil this goal (Hock *et al.*, 2017; [Nienow \*et al.\*, 2017](#)), although it usually involves trading-off either higher spatial resolution for lower temporal resolution, or vice versa. For example, the Landsat and ASTER satellites have been used to monitor lake evolution ([Sneed and Hamilton, 2007](#); [McMillan \*et al.\*, 2007](#); [Georgiou \*et al.\*, 2009](#); [Arnold \*et al.\*, 2014](#); [Banwell \*et al.\*, 2014](#); [Legleiter \*et al.\*, 2014](#); [Moussavi \*et al.\*, 2016](#); [Pope \*et al.\*, 2016](#); [Chen \*et al.\*, 2017](#); [Miles \*et al.\*, 2017](#); [Gledhill and Williamson, 2018](#); [Macdonald \*et al.\*, in press](#) [2018](#)). While this work involves analysing lakes at spatial

80 resolutions of 30 or 15 m, respectively, the best temporal resolution that can be achieved using these satellites is ~4 days and is often much longer due to the satellites' orbital geometry and/or site-specific cloud cover, which can significantly affect the observational record on the GrIS (Selmes *et al.*, 2011; Williamson *et al.*, 2017). This presents an issue for identifying rapid lake drainage with confidence since hydrofracture usually occurs in hours ~~to days~~ (Das *et al.*, 2008; ~~Selmes *et al.*, 2011~~; Doyle *et al.*, 2013; Tedesco *et al.*, 2013). An alternative approach involves tracking lakes at high temporal (sub-daily) resolution but at lower spatial resolution (~250–500 m) using MODIS imagery (Box and Ski, 2007; Sundal *et al.*, 2009; Selmes *et al.*, 2011, 2013; Liang *et al.*, 2012; Johansson and Brown, 2013; Johansson *et al.*, 2013; Morriss *et al.*, 2013; Fitzpatrick *et al.*, 2014; Everett *et al.*, 2016; Williamson *et al.*, 2017, 2018). However, this lower spatial resolution means that lakes < 0.125 km<sup>2</sup> cannot be confidently resolved (Fitzpatrick *et al.*, 2014; Williamson *et al.*, 2017) and even lakes that exceed this size are often omitted from the satellite record (Leeson *et al.*, 2013; Williamson *et al.*, 2017).

85 Because of the problems associated with the [frequency or spatial resolution of these](#) satellite records, it has been suggested that greater insights into GrIS hydrology might be gained if the images from multiple satellites could be used simultaneously (Pope *et al.*, 2016). Miles *et al.* (2017) were the first to present such a record of lake observations in West Greenland, combining imagery from the Sentinel-1 [Synthetic Aperture Radar \(SAR\)](#) (hereafter “Sentinel-1”) and Landsat 8 [Operational Land Imager \(OLI\)](#) (hereafter “Landsat 8”) satellites, and developing a method for tracking lakes at high spatial (30 m) and temporal resolution (~3 days). Using Sentinel-1 imagery facilitated lake detection through clouds and in darkness, enabling, for example, lake freeze-over in the autumn to be studied. This approach permitted the identification of many more lake-drainage events than would have been possible if either set of imagery had been used individually, as well as the drainage of numerous small lakes that could not have been identified with MODIS imagery (Miles *et al.*, 2017). Monitoring all lakes, including the smaller ones, many of which may also drain rapidly by hydrofracture, is important since recent work shows that a key determinant on subglacial ~~=~~drainage development is the density of surface-to-bed moulins opened by hydrofracture, rather than the hydrofracture events themselves ([e.g.](#) Banwell *et al.*, 2016; Koziol *et al.*, 2017). However, since Miles *et al.* (2017) used radar imagery, lake water volumes could not be calculated, restricting the type of information that could be obtained.

100 The Sentinel-2 [Multispectral Instrument \(MSI\)](#) comprises the Sentinel-2A (launched in 2016) and Sentinel-2B (launched in 2017) satellites, which have 290 km swath widths, a combined 5-day revisit time at the equator (with an even shorter revisit time at the poles), and 10 m spatial resolution in the optical bands; Sentinel-2 also has a 12-bit radiometric resolution, the same as Landsat 8, which improves on earlier satellite records with their 8-bit (or lower) dynamic range. Within glaciology so far, Sentinel-2 data have been used for mapping valley-glacier extents (Kääb *et al.*, 2016; Paul *et al.*, 2016), monitoring changes to ice-dammed lakes (Kjeldsen *et al.*, 2017), and cross-comparing ice-albedo products (Naegeli *et al.*, 2017); this research indicates that Sentinel-2 can be reliably combined with Landsat 8 since they produce similar results. Thus, Sentinel-2 imagery offers great potential for determining the changing volumes of lakes on the GrIS, for resolving smaller lakes, and for calculating volumes with higher accuracy than is possible with MODIS (Williamson *et al.*, 2017).

110 In this study, our objective is to present an automatic method for monitoring the evolution and drainage of lakes on the GrIS using a combination of Sentinel-2 and Landsat 8 imagery, which will allow the mosaicking of a high spatial resolution (10–30 m) record, with a frequent revisit time (approaching that of MODIS), something only possible by using the two sets of imagery simultaneously. The objective is addressed using four aims, which are to:

1. Trial new methods for calculating lake areas, depths and volumes from Sentinel-2 imagery and assess their accuracy against Landsat 8 for two days of overlapping imagery [in 2016](#).
- 115 2. Apply the best methods for Sentinel-2 from (1), alongside ~~an~~ existing methods for calculating lake areas, depths and volumes for Landsat 8, to all of the available ~~summer~~ 2016 [melt season](#) (May–October) imagery for a large study site

(~12,000 km<sup>2</sup>) in West Greenland. The aim is to apply t~~hese methods are applied~~ within an automated lake-tracking algorithm to produce time series of water=volume measurements for each lake in the study region to show their seasonal evolution.

- 120
3. Identify lakes that drain rapidly (in < 4 days) using the automatic algorithm, separating these lakes into small (< 0.125 km<sup>2</sup>) and large ( $\geq 0.125$  km<sup>2</sup>) categories, based on whether they could be identified with MODIS.
  4. Quantify the runoff volumes routed into the GrIS both during the lake-drainage events themselves, and afterwards via moulins opened by hydrofracture, for the small and large lakes.

## 2 Data and methods

125 Here, we describe the study region (Sect. 2.1), the collection and pre-processing of the Landsat 8 and Sentinel-2 imagery (Sect. 2.2), the technique for delineating lake area (Sect. 2.3), the methods used to calculate lake depth and volume (Sect. 2.4), the approaches for automatically tracking lakes and identifying rapid lake drainage (Sect. 2.5), and the methods used to determine the runoff volumes that are routed into the GrIS's internal hydrological system ~~interior~~ following the opening of moulins by hydrofracture (Sect. 2.6).

### 130 2.1 Study region

Our analysis focuses on a ~12,000 km<sup>2</sup> area of West Greenland, extending ~110 km latitudinally and ~90 km from the ice margin, with this spatial extent chosen based on the full coverage of the original Sentinel-2 tiles (Fig. 1; Sect. 2.2.2). It is primarily a land-terminating sector of the ice sheet, extending from the Sermeq Avannarleg outlet, which is just north of Jakobshavn Isbræ, near Ilulissat, to just south of Store Glacier in the Ummannaq district. We chose this study location because

135 it is an area of high lake activity, having been the focus of many previous remote-sensing studies with which our results can be compared (e.g. Box and Ski, 2007; Selmes *et al.*, 2011; Fitzpatrick *et al.*, 2014; Miles *et al.*, 2017; Williamson *et al.*, 2017, 2018).

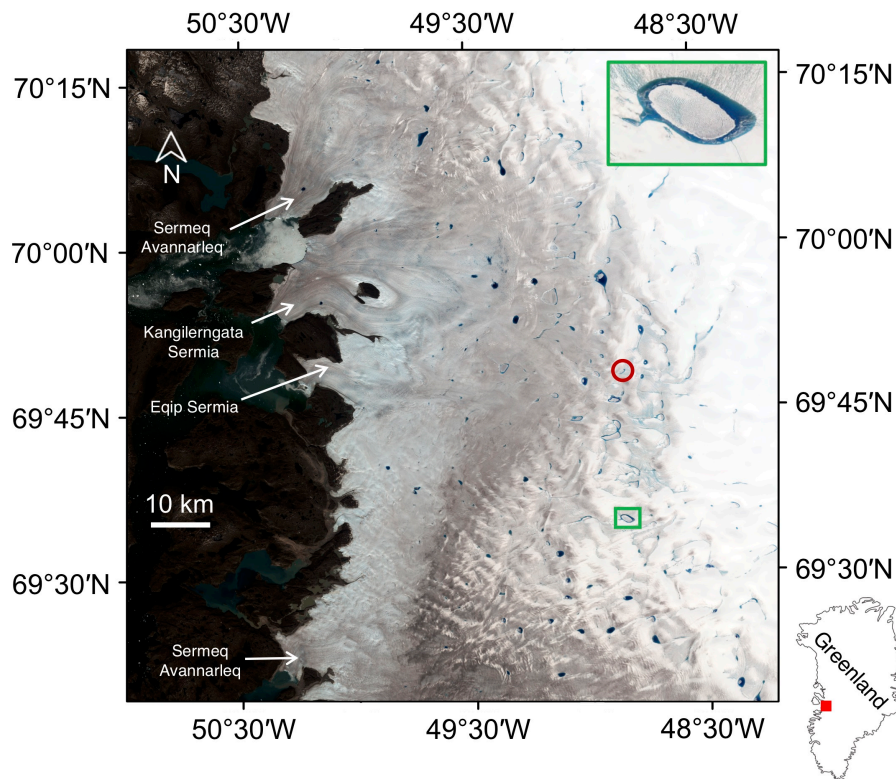


**Figure 1:** The ~12,000 km<sup>2</sup> study site within Greenland (inset). The background image is a Sentinel-2 RGB image from 11 July 2016 (see Table S1 for image details). [The green box and enlarged subplot](#) shows a rapidly draining lake and [the red circle](#) shows a non-rapidly draining lake (cf. Fig. 5).

## 2.2 Satellite imagery collection and pre-processing

### 2.2.1 Landsat 8

17 Landsat 8 images from May to October [2016](#) (Table S2) were downloaded from the USGS Earth Explorer interface (<http://earthexplorer.usgs.gov>). These were level-1T, radiometrically and geometrically corrected images, which were distributed as raw digital numbers. We required the 30 m resolution data from bands 2 (blue; 0.452–0.512  $\mu\text{m}$ ), 3 (green; 0.533–0.590  $\mu\text{m}$ ), 4 (red; 0.636–0.673  $\mu\text{m}$ ) and 6 (shortwave infrared ([SWIR](#)); 1.566–1.651  $\mu\text{m}$ ), and the 15 m resolution data from band 8 (panchromatic; 0.503–0.676  $\mu\text{m}$ ). We used all available 2016 imagery that covered at least a portion of the study site, regardless of cloud cover. Since Landsat 8 images cover greater areas than Sentinel-2 images, we batch cropped the Landsat 8 images to the extent of the Sentinel-2 images using ArcGIS's 'Extract by Mask' tool. All of the tiles were reprojected ([using bilinear resampling](#)) to the WGS 84 UTM 22N geographic coordinate system (EPSG: 32622) for consistency with the Sentinel-2 images, and ice-marginal areas were removed with the Greenland Ice Mapping Project (GIMP) ice-sheet mask (Howat *et al.*, 2014). The raw digital numbers were converted to top-of-atmosphere (TOA) reflectance using the image metadata and the USGS Landsat 8 equations (available at: <https://landsat.usgs.gov/landsat-8-18-data-users-handbook-section-5>). Landsat 8 TOA values adequately represent surface reflectance in Greenland (Pope *et al.*, 2016) and have been used previously for studying GrIS hydrology (Pope *et al.*, 2016; Miles *et al.*, 2017; Williamson *et al.*, 2017, 2018; Macdonald *et al.*, [in press 2018](#)). Our cloud-masking procedure involved marking pixels as cloudy when their band-6 ([SWIR](#)) TOA reflectance value exceeded 0.100 (Fig. 2), a method used for MODIS imagery albeit requiring a higher threshold value of 0.150 (Williamson *et al.*, 2017). We chose this lower threshold based on manual inspection of the pixels marked as cloudy against clouds visible on the original images. To reduce any uncertainty in the cloud-filtering technique, we then dilated the

cloud mask by 200 m (just over six Landsat 8 pixels), so that we could be confident that all clouds and their [nearby](#) shadows had been marked as ‘no data’ and would not affect the subsequent analyses. [The images were manually checked for shadowing elsewhere, with any shadows filtered where present.](#)

### 2.2.2 Sentinel-2

165 39 Sentinel-2A level-1C images from May to October [2016](#) (Table S1) were downloaded from the Amazon S3 Sentinel-2 database (<http://sentinel-s2-l1c.s3-website.eu-central-1.amazonaws.com>). The Sentinel-2 data were distributed as TOA reflectance values that were radiometrically and geometrically corrected, including ortho-rectification and spatial registration to a global reference system with sub-pixel accuracy. [We note that Sentinel-2 and Landsat 8 images are ortho-rectified using different DEMs, which may produce slight offsets in lake locations \(Kääb \*et al.\*, 2016; Paul \*et al.\*, 2016\); two contemporaneous](#)

170 [image pairs \(1 July and 31 July 2016\) were therefore manually checked prior to analysis, but no obvious offset was observed.](#) We included all Sentinel-2 images from 2016 that had  $\geq 20\%$  data cover of the study region and  $\leq 75\%$  cloud cover. This resulted in ~~the exclusion of 38 images from~~ [using 39 images from](#) the 77 in total available in 2016, reducing the average temporal resolution from 2.0 to 3.9 days. We downloaded data from Sentinel-2’s 10 m resolution bands 2 (blue; 0.460–0.520  $\mu\text{m}$ ), 3 (green; 0.534–0.582  $\mu\text{m}$ ) and 4 (red; 0.655–0.684  $\mu\text{m}$ ), and 20 m resolution data from band 11 (~~shortwave~~

175 ~~infrared~~[SWIR](#); 1.570–1.660  $\mu\text{m}$ ). Ice-marginal areas were removed using the GIMP ice-sheet mask (Howat *et al.*, 2014). We used a cloud-masking procedure similar to that for Landsat 8, where pixels were assumed to be clouds and were marked as ‘no data’ when the TOA value exceeded a threshold of 0.140 in band 11 ([SWIR](#)), after the band-11 data had been interpolated (using nearest-neighbour resampling) to 10 m resolution for consistency with the optical bands (Fig. 2). This threshold was chosen by manually comparing the pixels identified as clouds against background RGB images. As with the Landsat 8 images,

180 we diluted the cloud mask by 200 m (10 Sentinel-2 pixels) to account for any uncertainty in the cloud-masking procedure, [and again the images were manually checked for shadowing elsewhere, with any shadows filtered where present.](#)

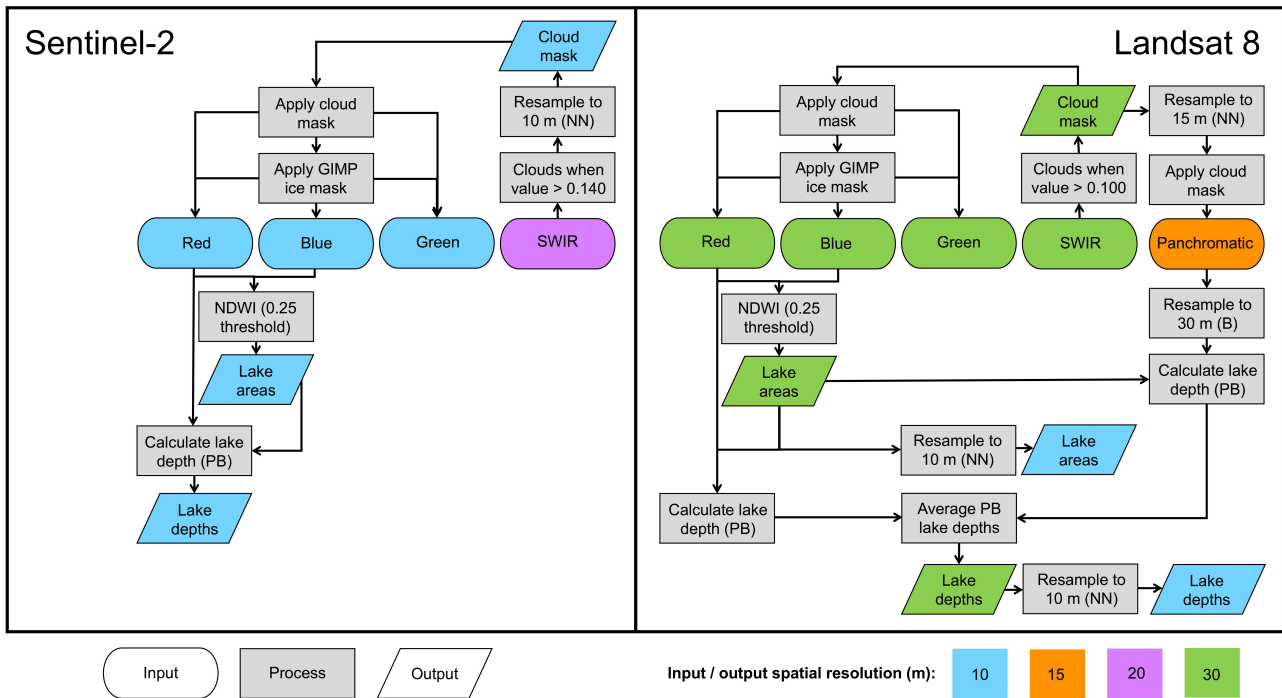


**Figure 2:** Summary of the methods applied to the Sentinel-2 and Landsat 8 input data to calculate lake areas using the NDWI and depths using the physically based (“PB” in this figure) method. In this figure, the interpolation techniques used are indicated by “NN” for nearest neighbour or “B” for bilinear. [The methods applied to Landsat 8 are shown only once the images had been reprojected and batch cropped to the same extent as the Sentinel-2 images \(Sect. 2.2.1\).](#) The lake-area outputs are compared between the two datasets as described in Sect. 2.3, and the physically based lake depth outputs are compared as outlined in Sect. 2.4. When the empirical lake depth method for calculating Sentinel-2 lake depths was also evaluated, the final Landsat 8 depths at 10 m resolution were directly compared against the original Sentinel-2 input band data (at native 10 m resolution) within the lake outlines defined from the NDWI.

### 2.3 Lake-area delineation

Figure 2 summarises the overall method used to calculate lake areas and depths for the Landsat 8 and Sentinel-2 imagery, including the cloud-masking procedure described above, and the resampling required because the data were distributed at different spatial resolutions. ~~Since the Landsat 8 optical band data were at 30 m native resolution, we first resampled them to 10 m resolution (using nearest-neighbour resampling) for consistency with the resolution of the Sentinel-2 data (Fig. 2).~~ We then derived lake areas for the two sets of imagery using the Normalised Difference Water Index (NDWI) approach, which has been widely used previously for medium- to high-resolution imagery of the GrIS (e.g. Moussavi *et al.*, 2016; Miles *et al.*, 2017). There were two stages involved here. First, we applied various NDWI thresholds to the Sentinel-2 and Landsat 8 images, and compared the delineated lake boundaries against the lake perimeters in the background RGB images. We then qualitatively selected the NDWI threshold for each type of imagery based on the threshold that produced the closest match between the two. Based on this qualitative analysis, we chose NDWI thresholds of 0.25 for both types of imagery (Fig. 2). By varying the thresholds in increments of  $\pm 0.01$  from these values [to 0.251 and 0.249, respectively](#), the total lake area calculated across the whole image only changed by  $< 2\%$ . The second stage involved comparing the areas of 594 lakes defined using the NDWI for the contemporaneous Landsat 8 and Sentinel-2 images from 1 July (collected in  $< 90$  minutes of each other) and 31 July (collected in  $< 45$  minutes of each other). This gave an extremely close agreement between the two sets of lake areas ( $R^2 = 0.999$ ; RMSE =  $0.007 \text{ km}^2$ , equivalent to seven Sentinel-2 pixels) without any bias, so we were confident that the NDWI approach applied to the two types of imagery reproduced the same lake areas (Fig. S1). Using these NDWI thresholds, we

created binary (lake and non-lake) masks for each day of imagery for the two satellites. [Since the Landsat 8 optical-band data were at 30 m native resolution, we resampled them to 10 m resolution \(using nearest-neighbour resampling\) for consistency with the resolution of the Sentinel-2 data \(Fig. 2\).](#) From the binary images, we removed groups of < 5 pixels in total and linear features < 2 pixels wide, since these were likely to represent areas of mixed slush or supraglacial streams, as opposed to lakes (Pope, 2016; Pope *et al.*, 2016).

## 2.4 Lake depth and volume estimates

### 2.4.1 Landsat 8

For each Landsat 8 image, we calculated the lake depths and volumes using the physically based method of Pope (2016) and Pope *et al.* (2016), based on Sneed and Hamilton's (2007) original method for ASTER imagery. This approach is based on the premise that there is a measurable change in the reflectance of a pixel within a lake according to its depth, since deeper water causes higher attenuation of the optical wavelengths within the water column. Lake depth ( $z$ ) can therefore be calculated based on the satellite-measured reflectance for a pixel of interest ( $R_{pix}$ ) and other lake properties:

$$z = \frac{[\ln (A_d - R_\infty) - \ln (R_{pix} - R_\infty)]}{g}, \quad (1)$$

where  $A_d$  is the lake-bottom albedo,  $R_\infty$  is the reflectance for optically deep (> 40 m) water, and  $g$  is the coefficient for the losses in upward and downward travel through a water column. For Landsat 8, we followed Pope *et al.*'s (2016) recommendation, taking an average of the depths calculated using the red and panchromatic band TOA reflectance data within the boundaries of the lakes (before they had been resampled to 10 m resolution for comparing the Sentinel-2 and Landsat 8 lake areas; Sect. 2.3) defined by the method described in Sect. 2.3. Since the panchromatic band data were at 15 m resolution, we resampled them using bilinear interpolation to match the 30 m red-band resolution (Fig. 2).  $A_d$  was calculated as the average reflectance in the relevant band for the ring of pixels immediately surrounding a lake,  $R_\infty$  was determined from optically deep water in proglacial fjords on a scene-by-scene basis for each band, and we used  $g$  values for the relevant Landsat 8 bands from Pope *et al.* (2016). Lake volume was calculated as the sum of lake depths, multiplied by the pixel area, within the lake outlines. We treated these Landsat 8 depths and volumes as ground-truth data as in Williamson *et al.* (2017).

### 2.4.2 Sentinel-2

Since no existing work has derived lake depths using Sentinel-2, we needed to formulate a new method. For this purpose, we used the Landsat 8 lake depths as our validation dataset. We conducted the validation on the two dates (1 July and 31 July 2016) with contemporaneous Landsat 8 and Sentinel-2 images (as described in Sect. 2.3). We chose to test both physically based and empirically based techniques to derive Sentinel-2 lake depths, noting at the outset that physical techniques are generally thought to be preferable over empirical ones since they do not require site- or time-specific tuning.

For the physically based technique, we tested whether the same method as applied to Landsat 8 (Eq. (1)) could be used on the Sentinel-2 TOA reflectance data. However, since Sentinel-2 does not collect panchromatic band measurements, we could only use [individual Sentinel-2's red bands](#) to calculate lake depths ([Fig. 2](#)). We applied this physically based technique to the red- [and green-band](#) data within the lake outlines defined with the NDWI (Sect. 2.3). We derived the value for  $R_\infty$  as described above for Landsat 8. [-but Since the lake-depth calculations are particularly sensitive to the  \$A\_d\$  value \(Pope \*et al.\*, 2016\), it was critical to ensure that the lake-bottom albedo was correctly identified. Thus, to define  \$A\_d\$ , we dilated the lake by a ring of two pixels, and not one, to ensure that shallow water was not included due to the finer pixel resolution and due to any errors in the lake outlines derived from the NDWI.](#) We also calculated [a new  \$g\$  values](#) for Sentinel-2's red [and green bands](#) using Pope *et al.*'s (2016) methods (Sect. S1).

Our empirically based approach involved deriving various lake depth-reflectance regression relationships (to determine which explained most variance in the data) using the Landsat 8 lake depth data (dependent variable) and the Sentinel-2 TOA reflectance data for the three optical bands (independent variables) for each pixel within the lake outlines predicted in both sets of imagery to determine which band and relationship produced the best match between the two datasets. To compare these values, we first resampled (using nearest-neighbour interpolation) the Landsat 8 depth data from 30 m to 10 m to match the resolution of the Sentinel-2 TOA reflectance data (Fig. 2).

To evaluate the performance of the empirical versus physical techniques, we calculated goodness-of-fit indicators for the Sentinel-2 and Landsat 8 measurements derived from the empirically based technique (applied to all optical bands) and physically based method (applied to the red [and green bands](#)) [for the two validation dates \(1 July and 31 July 2016\) when contemporaneous Landsat 8 and Sentinel-2 images were available](#).

As for Landsat 8, Sentinel-2 lake volumes were calculated as the sum of the individual lake depths, multiplied by the pixel areas, within the lake boundaries.

## 2.5 Lake evolution and rapid lake-drainage identification

### 2.5.1 Time series of lake water volumes

Once validated, the new techniques to calculate lake areas, depths and volumes from Sentinel-2, as well as the existing methods for Landsat 8 (Sect 2.4), were applied to the satellite imagery within the Fully Automated Supraglacial lake Tracking at Enhanced Resolution (FASTER) algorithm to produce cloud- and ice-marginal-free 10 m resolution lake area and depth arrays for each day of the 2016 melt season for which either a Landsat 8 or Sentinel-2 image was available (Fig. 2). For the days (1 July and 31 July) when both Landsat 8 and Sentinel-2 imagery was available (as used for the comparisons above), in the FASTER algorithm, we used only the higher-resolution Sentinel-2 images. The FASTER algorithm is an adapted version of the Fully Automated Supraglacial lake Tracking (FAST) algorithm (Williamson *et al.*, 2017), which was developed for MODIS imagery. The FASTER algorithm involves creating an array mask to show the maximum extent of lakes within the region in summer 2016, by superimposing the lake areas from each image. Within this maximum lake-extent mask, changes to lake areas and volumes were tracked between each consecutive image pair, with any lakes that were obscured (even partially) by cloud marked as 'no data'. We only tracked lakes that grew to  $\geq 495$  pixels (i.e.  $0.0495 \text{ km}^2$ ) at least once in the season, which is identical to the minimum threshold used by Miles *et al.* (2017), and is based on the minimum estimated lake size (approximated as a circle) required to force a fracture to the ice-sheet bed (Krawczynski *et al.*, 2009). It is encouraging that this minimum threshold size for lake tracking was over seven times larger than the error ( $0.007 \text{ km}^2$ ) associated with calculating lake area (Sect. 2.3; Fig. S1). While a lower tracking threshold could have been used, it would have significantly increased computational time and power required, alongside adding uncertainty to whether the tracked groups of pixels actually represented lakes. This tracking procedure produced time series for all lakes to show their evolution over the whole 2016 melt season.

### 2.5.2 Rapid lake-drainage identification

From the time series, a lake was classified as draining rapidly if two criteria were met: (i) it lost  $> 80\%$  of its maximum seasonal volume in  $\leq 4$  days (following Doyle *et al.*, 2013; Fitzpatrick *et al.*, 2014; Miles *et al.*, 2017; Williamson *et al.*, 2017, 2018); and (ii) it did not then refill on the subsequent day of cloud-free imagery by  $> 20\%$  of the total water volume lost during the previous time period (following Miles *et al.*, 2017); the aim here was to filter false positives from the record. However, we also tested the sensitivity of the rapid lake-drainage identification methodology by varying the threshold by  $\pm 10\%$  (i.e. 70–

90%) for the critical-volume-loss threshold,  $\pm 10\%$  (i.e. 10–30%) for the critical-refilling threshold, and  $\pm 1$  day (i.e. 3–5 days) for the critical-timing threshold.

To determine how much extra information could be obtained from the finer spatial resolution satellite record, we compared the number of rapidly draining lakes identified that grew to  $\geq 0.125$  km<sup>2</sup> (which would be resolvable by MODIS) with the number that never grew to this size (which would not be resolvable by MODIS) at least once in the season. We defined the drainage date as the midpoint between the date of drainage initiation and cessation, and identified the drainage date as half of this value. We conducted three sets of analyses: one for each set of imagery individually, and a third for both sets together; the intention here was to quantify how mosaicking the dual-satellite record improved the identification of lake-drainage events compared with using either record alone. The water volumes reaching the GrIS's internal hydrological system from the small and large lakes during the drainage events themselves were determined using the lake volume measurements on the day of drainage.

## 2.6 ~~Meltwater~~ Runoff deliveries following moulin opening

Using the dual Sentinel-2 and Landsat 8 record, the locations and timings of moulin openings by ‘large’ and ‘small’ rapidly draining lakes were identified. Then, at these moulin locations, the meltwater runoff volumes that subsequently entered the ice sheet were determined using statistically downscaled daily 1 km resolution RACMO2.3p2 runoff data (Noël *et al.*, 2018). Here, “runoff” was defined as melt plus rainfall minus any refreezing in snow (Noël *et al.*, 2018). These data were reprojected from Polar Stereographic (EPSG: 3413) to WGS 84 UTM zone 22N (EPSG: 32622) for consistency with the other data, and upsampled to 100 m resolution using bilinear resampling. Then, the ice-surface catchment for each rapidly draining lake was delineated using MATLAB’s ‘watershed’ function, applied to the GIMP ice-surface-elevation data (Howat *et al.*, 2014). The elevation data were first coarsened using bilinear resampling to 100 m resolution from 30 m native resolution. For each of the days after rapid lake drainage had finished, it was assumed that all of the runoff within a lake’s catchment reached the moulin in that catchment instantaneously (i.e. no flow-delay algorithm was applied) and entered the GrIS. This method therefore assumes that once a moulin has opened at a lake-drainage site, it remains open for the remainder of the melt season. This allowed first-order comparisons between cumulative runoff into the GrIS via the moulins opened by small and large lake-drainage events.

## 3 Results

### 3.1 Sentinel-2 lake-depth estimates

Table 1 shows the results of the lake-depth calculations using the physically and empirically based techniques applied to imagery from 1 July and 31 July 2016 when contemporaneous Landsat 8 and Sentinel-2 images were available. The physically based method (Figs. 3 and S2) applied to the red and green bands performed slightly less well (for the red band:  $R^2 = 0.841$  and RMSE = 0.555 m; for the green band:  $R^2 = 0.876$  and RMSE = 0.488 m) than the best empirical method (Fig. 4) when a power-law regression was applied to the data ( $R^2 = 0.889$  and RMSE = 0.447 m). Figures S3 and S4 respectively show the data for the empirical technique applied to the Sentinel-2 TOA reflectance and Landsat 8 lake depths for the more poorly performing Sentinel-2 green and blue bands (Table 1). The physically based method applied to the red-band data performed better on 1 July, where the relationship between Sentinel-2-derived depths and Landsat 8 depths was more linear (Fig. 3, blue markers) than on 31 July (Fig. 3, red markers), where the relationship was more curvilinear. This is because the depths calculated with Sentinel-2 on 31 July were limited to  $\sim 3.5$  m, while higher depths ( $> 4$  m) were reported on 1 July (Fig. 3). Although less distinct, the best empirical relationship also differed slightly in performance between the two dates (Fig. 4). Section 4.1 discusses the possible reasons for the under-measurement of lake depths with Sentinel-2 on 31

July compared with 1 July. The physically based method applied to the green-band data performed similarly on both validation dates (Fig. S2). Although application of the physically based technique to the green band produced a slightly higher R<sup>2</sup> and lower RMSE compared with the physically based method applied to the red-band data, the depths estimated with Sentinel-2 were unrealistically high compared with those from Landsat 8: Sentinel-2 reports a maximum depth of ~19 m, comparing with an equivalent value of ~5.5 m for Landsat 8 (Fig. S2). This produced a higher value for the sum of squares due to error (SSE) for the green band than the red band physical method (Table 1).

Although the physically based method performed slightly ~~more poorly~~ worse than the empirical techniques, the physical method is preferable because it can be applied across wide areas of the GrIS and in different years without site- or time-specific tuning; it is likely that a different empirical relationship would have better represented the data for a different area of the GrIS or in a different year. We therefore carried forward the physically based method applied to the red band into the lake-tracking approach. We selected the red band instead of the green band because of the large difference between the depths calculated with the two satellites at higher values when using the green band. We defined ~~ing~~ the error on all of the subsequently calculated lake ~~=~~ depth (and therefore lake ~~=~~ volume) measurements for Sentinel-2 using the RMSE of 0.555 m, and ~~treating~~ treated the Landsat 8 measurements as ground-truth data, meaning they did not have errors associated with them.

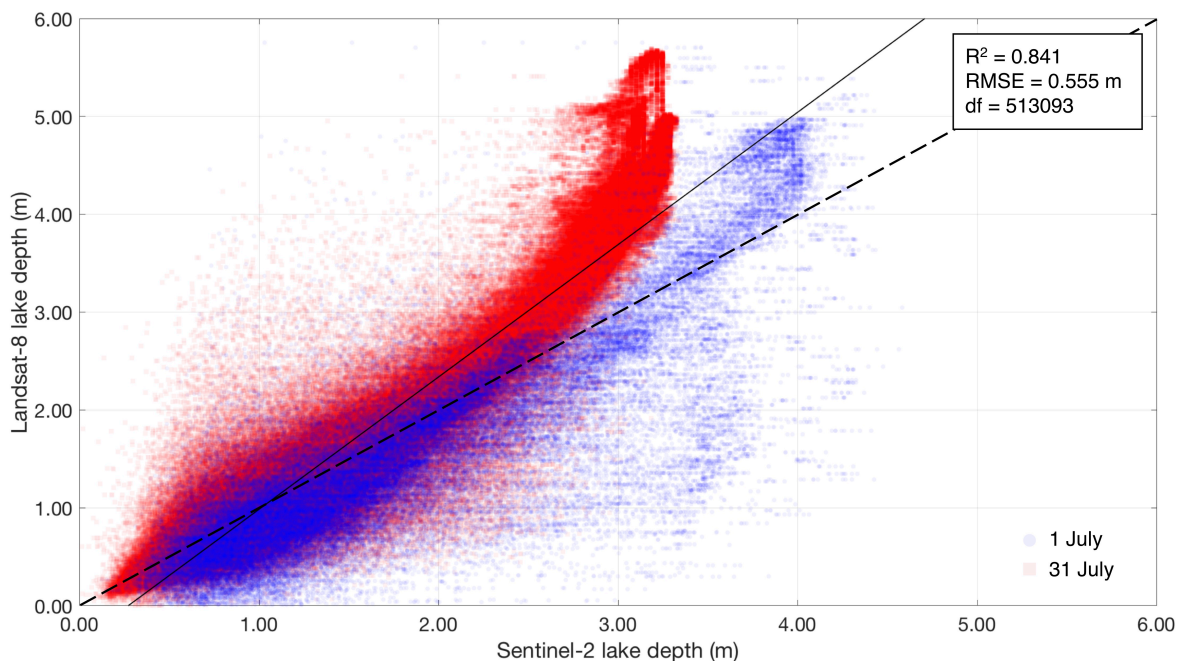
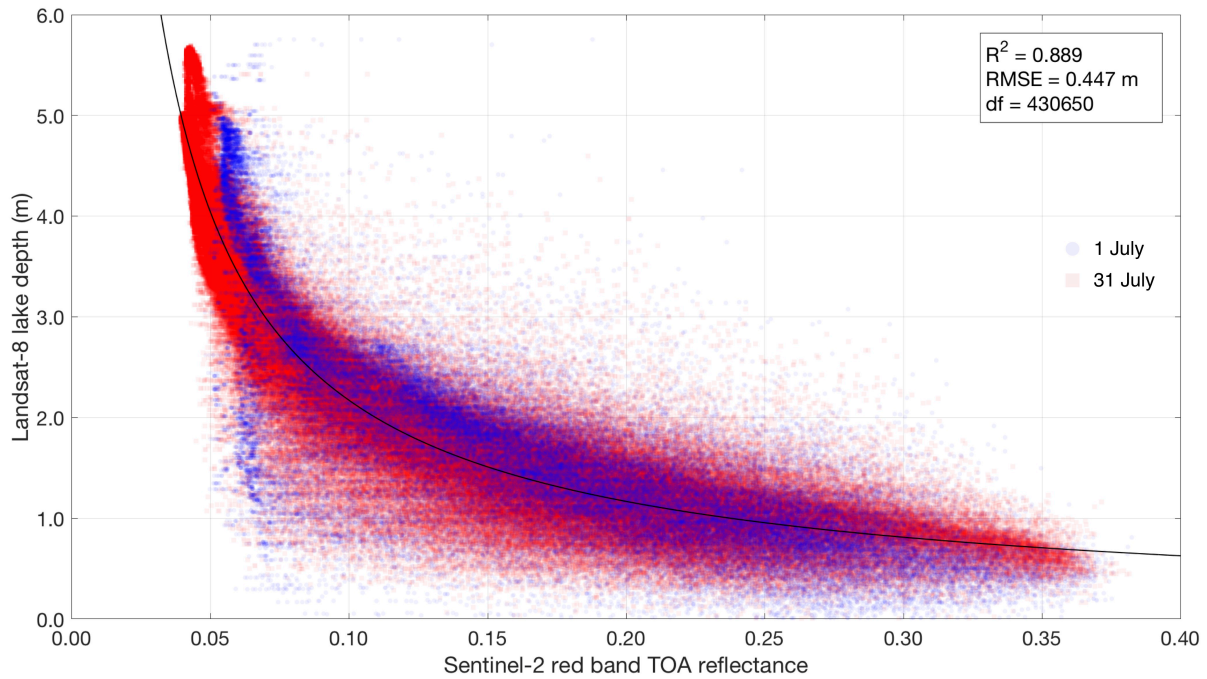


**Figure 3:** Comparison ~~between of~~ lake depths calculated using the physically based method for Sentinel-2 (with the red band) and for Landsat 8 (with the average depths from the red and panchromatic bands). Degrees of freedom (“df” in this figure) = 513,093 (~~blue circles = 1 July; red squares = 31 July~~). The solid black line shows an ordinary least-squares (OLS) linear regression and the dashed black line shows a 1:1 relation. The R<sup>2</sup> value indicates that the regression explains 84.1% of the variance in the data. The RMSE of 0.555 m shows the error associated with calculating the Sentinel-2 lake depths using this relationship.



345 **Figure 4:** The empirical power law regression (solid black curve, equation  $y = 0.2764x^{-0.8952}$ ) between Sentinel-2 red band TOA reflectance and Landsat 8 lake depth. Degrees of freedom ([“df” in this figure](#)) = 430,650 (~~blue circles = 1 July; red squares = 31 July~~). The  $R^2$  value indicates that the regression explains 88.9% of the variance in the data. The RMSE of 0.447 m shows the error associated with calculating the Sentinel-2 lake depths using this relationship.

350 **Table 1:** Goodness-of-fit indicators for the empirical and physical techniques tested in this study for deriving Sentinel-2 lake depths, with validation against the Landsat 8 lake depth measurements, [on 1 July and 31 July 2016](#).  $R^2$  is the coefficient of determination, RMSE is the root mean square error, and SSE is the sum of squares due to error. The best performing (red band) regression relationship (i.e. the one with highest  $R^2$ , and lowest RMSE and SSE) among the empirical techniques is shown in bold italicised text. [Data for the physical relation applied to Sentinel-2’s green band are presented in Fig. S2, and](#) [data for the empirical relation applied to Sentinel-2’s green and blue bands are presented in Figs. S32 and S43, respectively.](#)

| Sentinel-2 band (technique)      | Goodness-of-fit indicator           | OLS regression                        | Power-law regression                        | Exponential regression |
|----------------------------------|-------------------------------------|---------------------------------------|---|------------------------|
| Red (empirical)                  | $R^2$                               | 0.702                                 | <b><i>0.889</i></b>                         | 0.842                  |
|                                  | RMSE                                | 0.734                                 | <b><i>0.448</i></b>                         | 0.534                  |
|                                  | SSE (m <sup>3</sup> )               | $2.39 \times 10^5$                    | <b><i><math>8.62 \times 10^4</math></i></b> | $1.23 \times 10^5$     |
| Green (empirical)                | $R^2$                               | 0.782                                 | 0.768                                       | 0.829                  |
|                                  | RMSE                                | 0.627                                 | 0.647                                       | 0.556                  |
|                                  | SSE (m <sup>3</sup> )               | $1.69 \times 10^5$                    | $1.80 \times 10^5$                          | $1.33 \times 10^5$     |
| Blue (empirical)                 | $R^2$                               | 0.647                                 | 0.622                                       | 0.673                  |
|                                  | RMSE                                | 0.799                                 | 0.826                                       | 0.768                  |
|                                  | SSE (m <sup>3</sup> )               | $2.75 \times 10^5$                    | $2.94 \times 10^5$                          | $2.54 \times 10^5$     |
| Red (physical)                   | $R^2$                               | 0.841                                 | –   | –                      |
|                                  | RMSE                                | 0.555                                 | –   | –                      |
|                                  | SSE (m <sup>3</sup> )               | $1.58 \times 10^5$                    | –   | –                      |
| <a href="#">Green (physical)</a> | <a href="#">R<sup>2</sup></a>       | <a href="#">0.876</a>                 | =   | =                      |
|                                  | <a href="#">RMSE</a>                | <a href="#">0.488</a>                 | =   | =                      |
|                                  | <a href="#">SSE (m<sup>3</sup>)</a> | <a href="#">1.22 × 10<sup>5</sup></a> | =   | =                      |

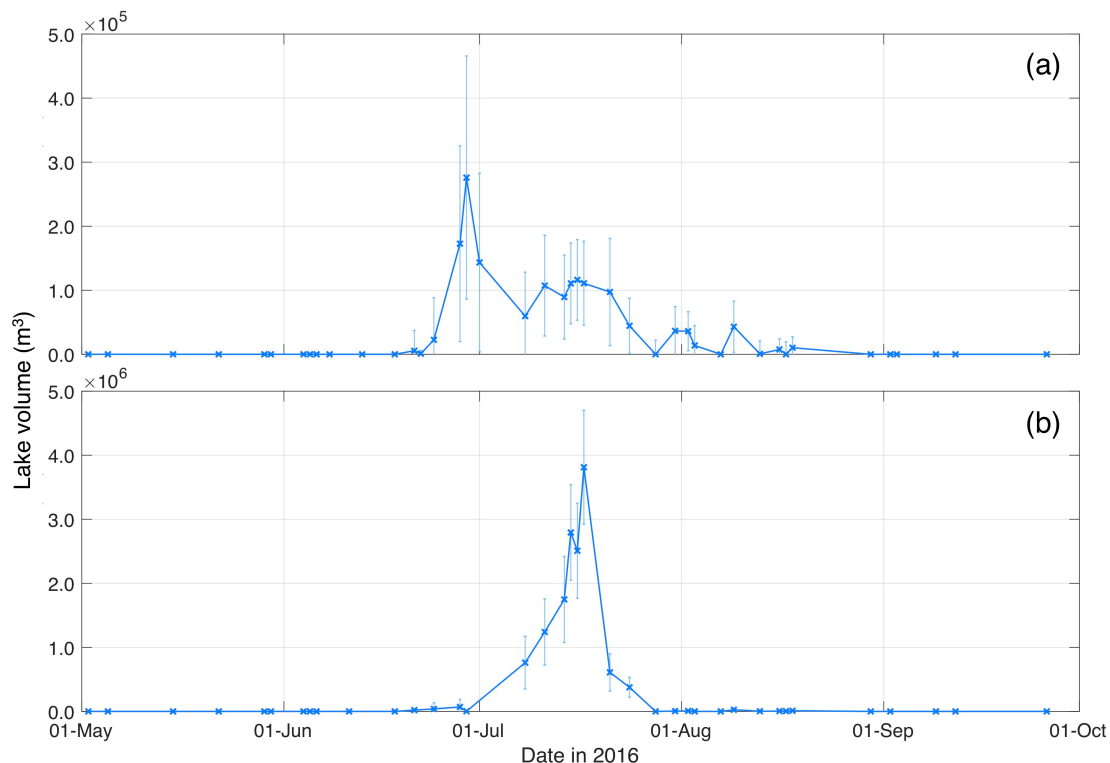
355

### 3.2 Lake evolution

Having verified the reliability of the lake area and depth techniques for both Sentinel-2 and Landsat 8, the automatic calculation methods were included in the FASTER algorithm to derive seasonal changes to lake areas and depths, and therefore volumes. The FASTER algorithm was applied to the Landsat 8 and Sentinel-2 image batches individually, as well as to both sets when  
360 combined into a dual record. Using the dual-satellite image collection produced an improvement to the temporal resolution of the dataset over the summer season (1 May to 30 September) from averages of 9.0 days (for Landsat 8) and 3.9 days (for Sentinel-2) to 2.8 days (for the dual record). The months of June and July had the most imagery available (both with 14 images) within the dual-satellite analysis. For the Landsat 8 individual analysis, the algorithm tracked changes to 453 lakes that grew to  $\geq 0.0495 \text{ km}^2$  once in the season; equivalent numbers were 599 lakes for the Sentinel-2 analysis, and 690 lakes for the dual-  
365 satellite analysis. Using the dual record therefore involved tracking an additional 237 (or 91) lakes over the season than was possible with Landsat 8 (or Sentinel-2) alone.

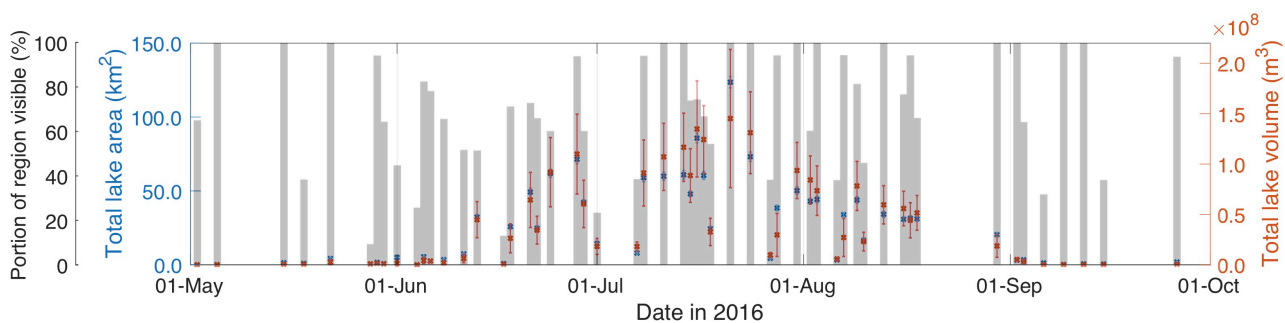
The largest lake size varied between the analyses:  $4.0 \text{ km}^2$  for Landsat 8 (recorded on 16 July 2016), and  $8.6 \text{ km}^2$  for Sentinel-2 (recorded on 21 July 2016), which may be because there ~~were~~ no Landsat 8 images close to 21 July 2016. The maximum lake volumes recorded also varied between the two platforms:  $1.1 \times 10^7 \text{ m}^3$  for Landsat 8 (recorded on 15 July  
370 2016) and  $1.2 \times 10^7 \text{ m}^3$  for Sentinel-2 (recorded on 14 July 2016). The mean ~~and median~~ lake sizes across all of the images from the dual Sentinel-2–Landsat 8 record ~~were  $0.09$  and  $0.137 \text{ km}^2$ , respectively~~ (25<sup>th</sup> and 75<sup>th</sup> percentiles =  $0.0075 \text{ km}^2$  and  $0.129 \text{ km}^2$ , respectively). ~~Both values~~ This value is therefore just above ~~were well below~~ (by  $0.01235 \text{ km}^2$  and  $0.105 \text{ km}^2$ , respectively) the threshold reporting size of MODIS, assuming two 250 m MODIS pixels are required to confidently classify lakes (Fitzpatrick *et al.*, 2014; Williamson *et al.*, 2017). Unpaired Student's *t*-tests between Sentinel-2 and Landsat 8  
375 lake areas and volumes (from all of the imagery) confirmed that they were not significantly different with > 99% confidence ( $t = 6.5$ , degrees of freedom = 9503 for areas;  $t = 11.4$ , degrees of freedom = 6859 for volumes), justifying using the two imagery types together despite their resolution difference (10 m versus 30 m).

Using the full Sentinel-2–Landsat 8 dataset, the FASTER algorithm produced time series that documented changes to individual lake volumes over the season, samples of which are shown in Fig. 5. Total areal and volumetric changes across the  
380 whole region were calculated by summing the values for all lakes in the region. However, we found that cloud cover (which was masked from the images) often affected the observational record, and there were time periods, such as early July and the end of August ~~and early July~~, with a lot of missing data (Fig. 6). Figure 7 was therefore produced to normalise total lake areas and volumes against the proportion of the region visible, and this shows the estimated pattern of lake evolution on the GrIS: ~~There~~ was virtually no water in lakes before June, steady increases in total lake area and volume until the middle of July, and  
385 then a gradual decrease in total lake area and volume through the remainder of the season, with most lakes emptying by early September (Figs. 6 and 7). Dates with seemingly low total lake areas and volumes were usually explained by the low portion of the whole region visible in those images (Figs. 6 and 7). Finally, as in previous studies (e.g. Box and Ski, 2007; Georgiou *et al.*, 2009; Williamson *et al.*, 2017), we found a close correspondence between lake areas and volumes: comparing lake area and volume values from all dates produced an  $R^2$  value of 0.73 ( $p = ~~0.00~~  $1.03 \times 10^{-10}$$ ).



390

**Figure 5:** Sample time series of lake volume to show seasonal changes for (a) a non-rapidly draining lake (Fig. 1, red circle) and (b) a rapidly draining lake (Fig. 1, green box). Lines connect points without any data smoothing. [Error bars were calculated by multiplying the lake-depth RMSE of 0.555 m by the pixel size and the number of pixels in the lake on each image.](#)



395

**Figure 6:** Evolution to total lake area and volume across the whole study region during the 2016 melt season. “Portion of region visible” measures the percentage of all of the pixels within the entire region that are visible in the satellite image, i.e. which are not obscured either by cloud (or cloud shadows) or are not missing data values. Figure 7 presents total lake area and volume after normalising for the proportion of region visible. [Blue error bars for lake area were calculated by multiplying the lake-area RMSE of 0.007 km<sup>2</sup> by the number of lakes identified on each image; red error bars for total lake volume were calculated by multiplying the lake-depth RMSE of 0.555 m by the pixel size and the number of pixels identified to be water-covered on each image.](#)

400

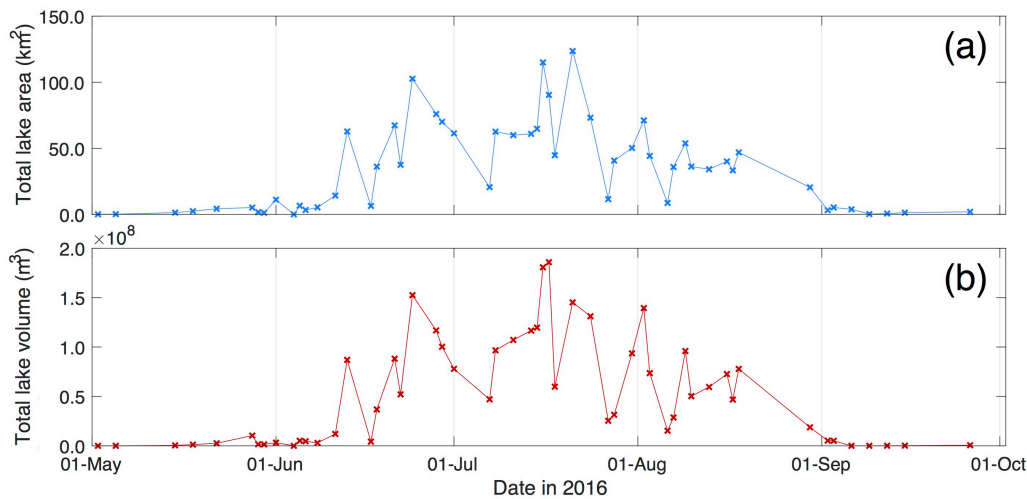


**Figure 7:** Estimates of evolution to total lake (a) area and (b) volume across the whole study region during the 2016 melt season after daily values were normalised against the proportion of the region visible of the region visible on that day (i.e. not obscured by cloud or missing data). Values are derived by dividing the daily total lake area and volume by the portion of the region visible on that day (cf. Fig. 6).

### 3.3 Rapid lake drainage

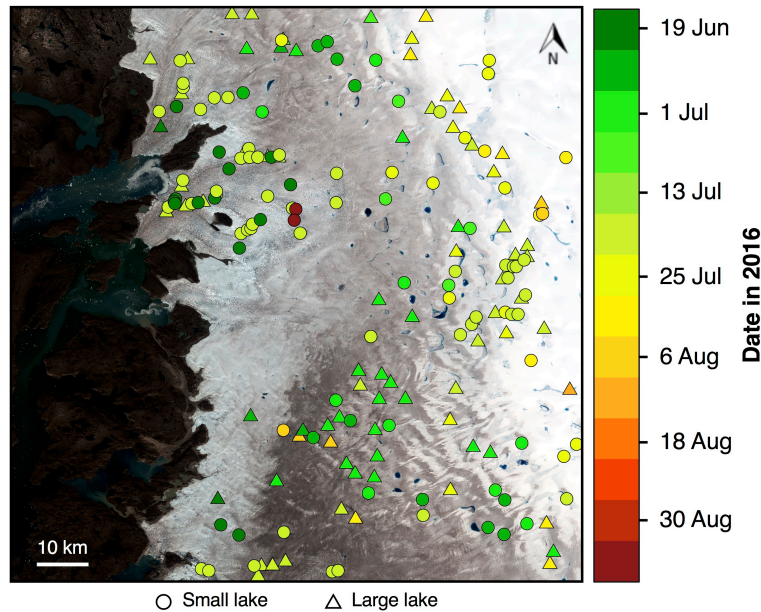
Table 2 shows the results of the identification of rapidly draining lakes using the three different datasets, and indicates that the dual-satellite record was better for identifying rapidly draining lakes than the individual records. This was for two main reasons. First, the dual-satellite record identified 118 (or 91) additional rapidly draining lakes than the Landsat 8 (or Sentinel-2) record in isolation (Table 2). When either record was used alone, Sentinel-2 (or Landsat 8) performed better (or worse), identifying 50.5% (or 35.9%) of the total number of rapidly draining lakes identified by the dual-satellite record. Second, with the dual-satellite dataset, drainage dates were identified with ~~lower error~~ higher precision (i.e. half of the number of days between the date of drainage initiation and cessation; Sect. 2.5.2) than with the Sentinel-2 analysis (Table 2). However, the ~~precision errors~~ appears ~~lower~~ higher for the Landsat 8 analysis than either the dual-satellite or Sentinel-2 analysis, and this is because nearly all Landsat 8 lake-drainage events occurred on two occasions when ~~the pair of images~~ ~~an image pair~~ was only separated by a day, on 8–9 July (small lakes) and 13–14 July (large lakes) (Table 2).

The dual-satellite record also identified the rapid drainage of many small lakes (< 0.125 km<sup>2</sup>) that would not be visible with MODIS imagery due to the lower limit of its reporting size (Table 2), thus presenting an advantage of the dual-satellite record over the MODIS record of GrIS surface hydrology. These smaller lakes tended to drain rapidly earlier in the season (mean date = 8 July for the dual-satellite record) than the larger lakes (mean date = 11 July for the dual-satellite record), although the difference in dates is small, with most lakes draining in early to mid-July (Table 2; Fig. 8). In general, lakes closer to the ice margin tended to drain earlier than those inland (Fig. 8).

Finally, we tested how adjusting the thresholds used to define rapidly draining lakes would impact rapid lake-drainage identification. Changing the critical volume loss required for a lake to be identified as having drained from 80% to 70% and 90% resulted in the identification of only six more and four fewer rapid lake-drainage events, respectively. Similarly, changing the critical-refilling threshold from 20% to 10% and 30% resulted in identifying only eight fewer and five more rapidly draining lakes. However, adjusting the timing over which this loss was required had a larger impact, with adjustments from 4 to 3 and 5 days producing 37 fewer and 65 more rapid lake-drainage events, respectively.

430 **Table 2:** Properties of rapid lake-drainage events identified using the satellite datasets individually and when as part of a dual-satellite dataset. Large lakes are [defined as](#)  $\geq 0.125$  km<sup>2</sup> (identifiable by MODIS), while small lakes are [defined as](#)  $< 0.125$  km<sup>2</sup> (omitted by MODIS). “DoY” refers to day of year in 2016.

| Analysis type   | Property   | Large lakes     | Small lakes     | Total/overall   |
|---|--|-----------------|-----------------|-----------------|
| Sentinel-2  | Number of drainage events                                      | 45              | 48              | 93              |
|   | Percentage of total lakes                                      | 7.5             | 8.0             | 15.5            |
|   | Mean drainage date (DoY) $\pm$ mean <del>error</del> precision | 193.4 $\pm$ 1.8 | 188.2 $\pm$ 1.6 | 190.7 $\pm$ 1.7 |
|   | Minimum drainage volume (10 <sup>5</sup> m <sup>3</sup> )      | 0.020           | 0.006           | 0.006           |
|   | Maximum drainage volume (10 <sup>5</sup> m <sup>3</sup> )      | 90.1            | 2.1             | 90.1            |
|   | Mean drainage volume (10 <sup>5</sup> m <sup>3</sup> )         | 7.5             | 0.2             | 3.7             |
|   | Median drainage volume (10 <sup>5</sup> m <sup>3</sup> )       | 1.3             | 0.2             | 0.3             |
|   | Total drainage volume (10 <sup>5</sup> m <sup>3</sup> )        | 337.3           | 11.7            | 349.0           |
| Landsat 8   | Number of drainage events                                      | 30              | 36              | 66              |
|   | Percentage of total lakes                                      | 6.6             | 7.9             | 14.6            |
|   | Mean drainage date (DoY) $\pm$ mean <del>error</del> precision | 196.8 $\pm$ 0.6 | 190.5 $\pm$ 0.5 | 193.4 $\pm$ 0.5 |
|   | Minimum drainage volume (10 <sup>5</sup> m <sup>3</sup> )      | 0.100           | 0.050           | 0.050           |
|   | Maximum drainage volume (10 <sup>5</sup> m <sup>3</sup> )      | 19.8            | 1.1             | 19.8            |
|   | Mean drainage volume (10 <sup>5</sup> m <sup>3</sup> )         | 4.2             | 0.4             | 2.1             |
|   | Median drainage volume (10 <sup>5</sup> m <sup>3</sup> )       | 1.6             | 0.4             | 0.6             |
| Total drainage volume (10 <sup>5</sup> m <sup>3</sup> ) | 126.8  | 14.1            | 140.9           |                 |
| Dual<br>Sentinel-2<br>and<br>Landsat 8                  | Number of drainage events                                      | 79              | 105             | 184             |
|   | Percentage of total lakes                                      | 11.4            | 15.2            | 26.7            |
|   | Mean drainage date (DoY) $\pm$ mean <del>error</del> precision | 193.1 $\pm$ 1.1 | 190.1 $\pm$ 1.0 | 191.4 $\pm$ 1.1 |
|   | Minimum drainage volume (10 <sup>5</sup> m <sup>3</sup> )      | 0.006           | 0.007           | 0.006           |
|   | Maximum drainage volume (10 <sup>5</sup> m <sup>3</sup> )      | 91.0            | 1.6             | 91.0            |
|   | Mean drainage volume (10 <sup>5</sup> m <sup>3</sup> )         | 7.4             | 0.3             | 3.4             |
|   | Median drainage volume (10 <sup>5</sup> m <sup>3</sup> )       | 1.8             | 0.2             | 3.9             |
| Total drainage volume (10 <sup>5</sup> m <sup>3</sup> ) | 586.1  | 31.2            | 617.3           |                 |



435 **Figure 8:** Dates of rapid drainage events for small (circles) and large (triangles) lakes in 2016. The panel coverage and background are the same as that shown in Fig. 1. The extreme colour bar values include those dates outside of the range shown (i.e. before 19 June and after 5 September, respectively).

### 3.4 ~~Meltwater~~ Runoff deliveries and moulin opening by rapid lake drainage

Each rapid lake-drainage event from the dual-satellite record delivered a mean water volume of  $3.4 \times 10^5 \text{ m}^3$  (range =  $0.006\text{--}91.0 \times 10^5 \text{ m}^3$ ;  $\sigma = 10.2 \times 10^5 \text{ m}^3$ ) into the ice sheet (Table 2; Fig. 9). Figure 9 shows the patterns of ~~meltwater~~ runoff delivery across the region, suggesting that small ( $< 0.125 \text{ km}^2$ ) and large ( $\geq 0.125 \text{ km}^2$ ) rapidly draining lakes weare randomly distributed across the region, although there were more numerous smaller lakes at lower elevations in the north. Figure 10 shows that large lakes generally contained ed more water than small lakes, as might be expected, but also shows that large lakes contained ed a higher range of water volumes than small lakes, producing an overlap between the lake types for the lower water volume values. Thus, although large lakes each covered ed a higher area, some large lakes must have been relatively shallow, as also suggested by the red to yellow coloured triangles on Fig. 9.

Using the data from the dual-satellite record, and considering just the water volumes delivered into the GrIS during lake-drainage events (and not subsequently via the moulins opened), the drainage of small ( $< 0.125 \text{ km}^2$ ) lakes delivered eds a total ~~meltwater~~ runoff volume of  $31.2 \times 10^5 \text{ m}^3$ , which is just 5.1% of the total volume ( $617.3 \times 10^5 \text{ m}^3$ ) delivered into the GrIS during the drainage of all lakes across the region (Table 2). Although this volume is low, small lake-drainage events, like large lake-drainage events, are additionally important because they are associated with the opening of moulins that transport surface ~~meltwater~~ runoff into the GrIS, and perhaps to the bed, for the remainder of the season, assuming that the moulin remains open (e.g. Banwell *et al.*, 2016; Koziol *et al.*, 2017). Associating lake drainages with moulin opening in this way means that the dual-satellite record found~~finds~~ an additional 105 moulins (Table 2) that would not have been identified by MODIS; this is greater than the total number of moulins associated with large lake-drainage events (79) that could have been identified by MODIS, assuming MODIS can identify all lakes  $> 0.125 \text{ km}^2$ , which itself is unlikely (Leeson *et al.*, 2013; Williamson *et al.*, 2017). Figure 11 shows that the moulins opened by the rapid drainage of small lakes allowed a higher total volume of ~~meltwater~~ runoff to enter the GrIS than that routed via moulins opened by rapidly draining large lakes; in total, moulins opened by small (large) lakes channelled  $1.61 \times 10^{16}$  ( $1.04 \times 10^{16}$ )  $\text{m}^3$  w.e. of ~~meltwater~~ runoff into the GrIS's internal hydrological system interior. Thus, moulins opened by small (large) lakes delivered 61.5% (38.5%) of the total runoff into the GrIS after opening.

Moreover, moulins opened by small lakes delivered more ~~meltwater runoff~~ into the GrIS than those opened by large lakes across all ice-elevation bands, although this finding is more pronounced at lower elevations than higher elevations, i.e. below and above 800 m a.s.l. respectively (Fig. 11). The runoff into the moulins opened by small lakes also tended ~~s~~ to reach the GrIS's ~~internal hydrological system~~ ~~interior~~ earlier in the season than that delivered into the moulins opened by large lakes, because these lakes tended to drain ~~slightly~~ earlier (Fig. 11).

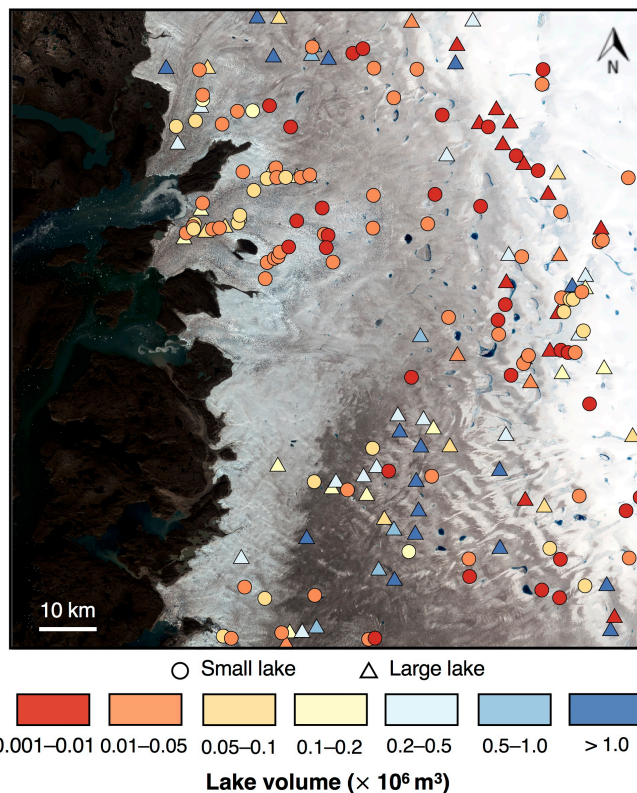


**Figure 9:** Lake water volumes measured using the physically based technique on the days prior to their rapid drainage, categorised into small (<math>< 0.125 \text{ km}^2</math> in area; circles) and large lakes (>math>\ge 0.125 \text{ km}^2</math> in area; triangles). Each point shown is also assumed to represent the location at which a moulin is opened by hydrofracture during rapid lake drainage, and which then remains open for the remainder of the season. The panel coverage and background are the same as that in Fig. 1.

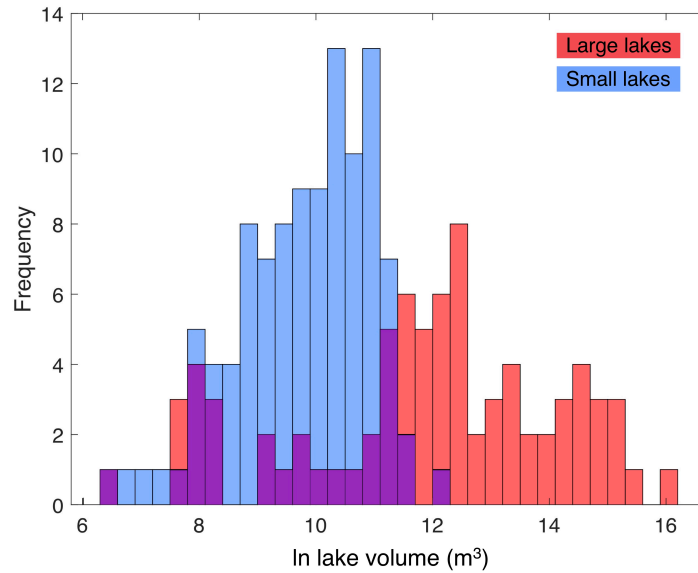
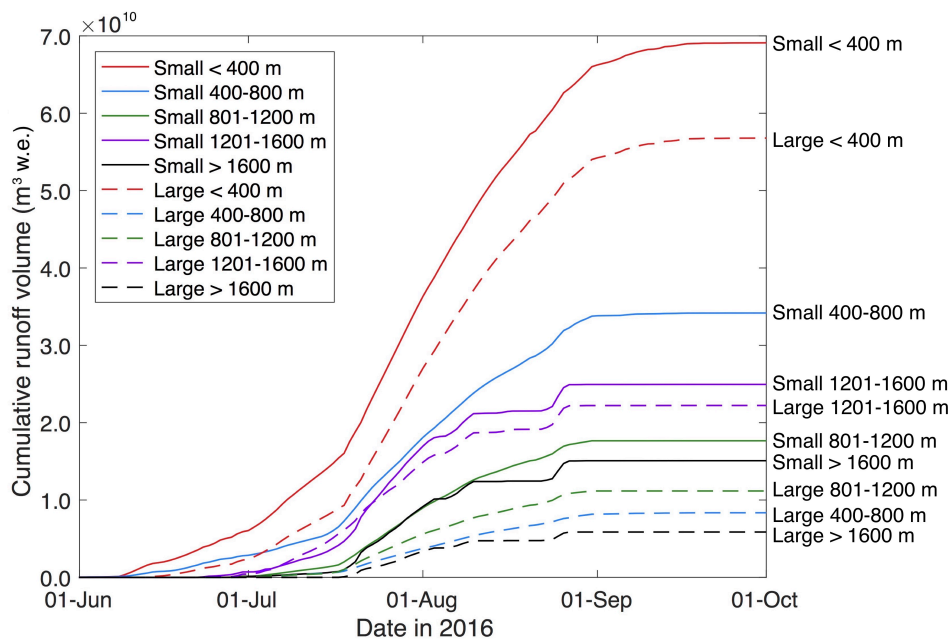


**Figure 10:** Frequency distribution of water volumes prior to rapid drainage for small and large lakes to show the lower and more tightly clustered water volumes contained within small lakes compared with large lakes. [Natural logs of  \$\ln\$  water volumes were log-normalised \(to the base 10\) taken for presentation purposes.](#)



475

**Figure 11:** Cumulative runoff volume,  $\times 10^{10}$  (from RACMO2.3p2 data (Noël *et al.*, 2018)) entering the GrIS over the remainder of the melt season via the moulines opened by rapid lake drainage for small ( $< 0.125 \text{ km}^2$ ) and large ( $\geq 0.125 \text{ km}^2$ ) lakes for different ice-surface-elevation bands,  $\times 10^3$  (derived from Howat *et al.* (2014)) shown in m a.s.l. in the legend and line labels. Runoff volume is derived within lakes' ice-surface catchments and is assumed to reach the moulin instantaneously on each day, without any flow delay.

480

## 4 Discussion

### 4.1 Sentinel-2 lake-depth estimates

The first and second aims of this study involved trialling and then applying a new method for calculating lake depths from Sentinel-2 imagery. We found an RMSE of 0.555 m ~~for~~ lake depths calculated with the physically based method applied to Sentinel-2's red band when compared with lake depths calculated from Landsat 8 using existing methods (Pope *et al.*, 2016).  
485 When we applied the physically based method to Sentinel-2's green band and compared the depths with Landsat 8 measurements, we found a slightly lower RMSE, but the Sentinel-2 depths were unrealistically high compared with Landsat 8 values, producing a high SSE, and so this method was excluded (Table 1; Fig. S2). We ~~opted~~ ~~selected~~ ~~for~~ the physical method over the empirical one because the empirical method cannot be applied without the site- or time-specific adjustments suggested  
490 in previous research (e.g. Sneed and Hamilton, 2007; Pope *et al.*, 2016; Williamson *et al.*, 2017), and might therefore perform more poorly in other years and/or for other regions of the GrIS. Given that the performance of the two methods was very similar, it therefore seemed most sensible to use the more robust physically based technique. In addition, the RMSE value (0.555 m) obtained here using the physically based method applied to the red band is only slightly higher than the error on lake-depth calculations using the physical method for similar-resolution Landsat 8 data (0.28 m for the red band and 0.63 m  
495 for the panchromatic band; Pope *et al.*, 2016). However, the RMSE on Sentinel-2 lake depths is less than half both that produced using the physically based method applied to coarser-resolution (250 m) MODIS red band data (1.27 m; Williamson *et al.*, 2017) and that produced using an empirical depth-reflectance relationship for MODIS (1.47 m; Fitzpatrick *et al.*, 2014). Therefore, using this record over MODIS imagery produces a much more reliable measure of lake-water depths on the GrIS because of the improved spatial resolution. The dual-satellite record is even further strengthened by its high temporal  
500 resolution, which approaches that of MODIS (Sect. 4.2).

Despite the low overall error for the physically based lake-depth calculations from Sentinel-2, we observed different performances on the two validation dates (1 July and 31 July; Sect. 3.1): the depths calculated for Sentinel-2 and Landsat 8 showed closer agreement on 1 July than on 31 July (Fig. 3). This is likely because clouds obscured a large portion of the image from 1 July. Although the lakes used for comparison were cloud-free and pixels within 200 m of a cloud-marked area were  
505 filtered, there were likely adjacency effects (at distances > 200 m from the clouds) associated with the cloud, which had more of an impact for Sentinel-2 than for Landsat 8. For example, the pixel brightness might have been reduced in locations relatively close to the clouds, consequently producing higher lake depths with the seemingly darker water (Fig. 3). Similar cloud adjacency effects have been recorded with other satellites, such as MODIS (Feng and Hu, 2016), and Landsat 8 and RapidEye (Houborg and McCabe, 2017). The depths calculated with the physical method on 31 July (Fig. 3), when there was less cloud  
510 cover, are therefore more likely to be *true* depths than the depths from 1 July when the image was affected by the cloud, even though the 1 July depths *appear* to be more correct. Assuming this is the case, our results indicate that Sentinel-2 may not ~~entirely~~ accurately record deeper water ( $> \sim 3.5$  m; Fig. 3) using the physical method applied to the red band. This is perhaps because the red wavelengths become saturated (i.e. fully attenuated) within the water column at higher depths, a result similar to that observed for lake-depth measurements from WorldView-2 and Landsat 8 (Moussavi *et al.*, 2016; Pope *et al.*, 2016; Williamson *et al.*, 2017). This is also likely to explain the lower maximum lake volume recorded in this study ( $1.2 \times 10^7$  m<sup>3</sup>) compared with previous work, such as the maximum lake volume of  $5.3 \times 10^7$  m<sup>3</sup> identified by Box and Ski (2007).  
515

Alternatively, the presence of clouds on the 1 July image might be indicative of a difference in the atmospheric composition on that day, which could have affected the lake-depth calculations with Sentinel-2, but not to the same degree with Landsat 8. This might be because of the difference in bandwidths between the satellites, or because Landsat 8's panchromatic band (used  
520 for calculating lake depths) is less sensitive to the presence of clouds in an image, therefore producing more reliable lake-depth

525 measurements. The effect of clouds on the atmosphere could have been better accounted for if our Sentinel-2 TOA reflectance data had been first converted to bottom-of-atmosphere (i.e. surface-reflectance) measurements. However, while surface-reflectance data are available for Landsat 8's optical bands, they are not for its panchromatic band, meaning that the lake-depth calculation method used here could not have been applied to generate reliable ground-truth data. We therefore intentionally chose not to perform this correction on the Sentinel-2 TOA data because we wished to directly compare the measurements from the two satellites.

530 Finally, in this study, the Sentinel-2 lake depths were validated using Landsat 8 measurements, which were regarded as ground-truth data, in line with a previous study involving validation of depths calculated with MODIS (Williamson *et al.*, 2017). This approach was justified since previous work (Pope *et al.*, 2016) indicated a close agreement between Landsat 8 lake depths and DEM measurements. However, it is important to note that the Landsat 8 data have errors associated with them, including a possible under-measurement of the deepest water due to saturation of the red band within the water column (Moussavi *et al.*, 2016; Pope *et al.*, 2016). Future work involving Sentinel-2 lake-depth calculations could therefore alternatively validate Sentinel-2 lake-depth estimates using different ground-truth validation data, such as higher-resolution (e.g. WorldView-2) satellite imagery, high-resolution DEM measurements of lake basins, or field lake-depth measurements.

## 535 4.2 Lake evolution

The second aim of this research was to apply the new methods for calculating lake areas, depths and volumes from Sentinel-2 imagery alongside those for Landsat 8 within the FASTER algorithm to produce time series for the evolution of all lakes. Applying this algorithm to the dual-satellite record allowed us to track the evolution of 690 lakes. The mean ~~and median~~ lake sizes (0.13709 km<sup>2</sup> ~~and 0.02 km<sup>2</sup>~~) ~~was~~ ~~ere well below~~ just above the threshold (0.125 km<sup>2</sup>) of lake size that MODIS can identify. Using a dual-satellite record, we were therefore able to achieve both high temporal (2.8 days) and spatial resolution (10–30 m). Previous studies (e.g. Selmes *et al.*, 2011, 2013; Fitzpatrick *et al.*, 2014; Miles *et al.*, 2017; Williamson *et al.*, 2017) have acknowledged that MODIS is useful because it can provide very high temporal resolution (up to sub-daily repeat site imaging) since the GrIS's surface hydrology can change quickly. However, because of the coarse spatial resolution, lake area and depth can only be calculated with large errors: for example, Williamson *et al.* (2017) calculate errors on MODIS lake areas of 0.323 km<sup>2</sup> (nearly ~~fifty~~ ~~six~~ times larger than the value derived in the present study) and on MODIS lake depths of 1.27 m (twice that obtained in this study). The minor loss of temporal resolution (i.e. a reduction from daily to 2.8 days) by using the dual-satellite record rather than MODIS is therefore ~~offset~~ overcome by the record's improved ~~accuracy~~ reliability for ~~in~~ resolving lake areas and depths. The use of Sentinel-2B data (available from 2017) alongside the Sentinel-2A data used here would allow further improvements to the dual record's temporal resolution; for example, in 2017, the temporal resolution of the Sentinel-2 data could be improved to an average of 1.4 days (if including all cloud-covered images) or 1.9 days (if excluding near-100% cloud-covered images) (Williamson, 2018a).

## 545 4.3 Rapid lake drainage

555 The third and fourth aims of the work were to identify the lakes tracked by the FASTER algorithm that drained rapidly, and to investigate the quantity of runoff reaching the GrIS's internal hydrological system ~~interior~~ both during the drainage events themselves and subsequently via the moulins opened by rapid lake drainage, since recent work (Banwell *et al.*, 2016; Koziol *et al.*, 2017) has shown that the moulins opened by rapid lake-drainage events allow much greater meltwater runoff volumes to reach the subglacial system than the actual drainage events themselves. Most research to date has used MODIS imagery to identify rapidly draining lakes because the high temporal resolution is required to separate rapidly draining lakes from those draining slowly. Although this MODIS-based research has been helpful for quantifying the characteristics of relatively large

560 lakes ( $\geq 0.125 \text{ km}^2$ ) and the potential controls on their rapid drainage (Box and Ski, 2007; Morriss *et al.*, 2013; Fitzpatrick *et al.*, 2014; Williamson *et al.*, 2017, 2018), such work has been unable to study smaller ( $< 0.125 \text{ km}^2$ ) lakes.

Rapid drainage of both large and small lakes can be identified using the FASTER algorithm with the dual-satellite record. Although the water volumes associated with the drainage of small lakes into the GrIS amount to just 5.1% of the total water volume associated with the drainage of all lakes across the region, rapid drainage of small lakes is important because, like  
565 large lakes, they open ~~up~~ moulins that can direct surface ~~meltwater runoff~~ into the GrIS's ~~internal hydrological system interior~~ over the remainder of the season (~~Banwell *et al.*, 2016; Koziol *et al.*, 2017~~). This assumes that the moulins remain open for the rest of the melt season, and we note that this may vary across the study region according to ice thickness or stress state. However, acknowledging this assumption, ~~W~~with the dual-satellite record, we identified 105 small rapid lake-drainage events, thus providing 105 additional input ~~locations~~ for surface ~~meltwater runoff~~ to reach the ice ~~sheet's internal hydrological system interior~~  
570 ~~system interior~~ than would be identified by MODIS. The moulins opened by small lake-drainage events are particularly important because in total they deliver over half (61.5%) of the total ~~meltwater runoff~~ delivered via all moulins into the GrIS's ~~internal hydrological system interior~~. This is because the small rapidly draining lakes are more numerous (105 compared with 79) and tend to be at lower elevations than the larger lakes (small lake mean elevation = 697 m a.s.l. and  $\sigma = 514 \text{ m a.s.l.}$ ; large lake mean elevation = 848 m a.s.l. and  $\sigma = 563 \text{ m a.s.l.}$ ), where surface melting is higher. Moreover, small lakes tend to drain slightly earlier in the melt season (Table 2), meaning that the moulins they ~~create are~~ open can receive runoff for a slightly greater proportion of the melt season, ~~and because smaller lakes tend to be at lower elevations than the larger lakes, where surface melting is higher~~. In addition, the moulins opened by small lake-drainage events tend to result in higher volumes of runoff reaching the GrIS's ~~internal hydrological system interior~~ earlier rather than later in the season (Fig. 11), which may be important because the subglacial system is likely to be less hydraulically efficient at this time (e.g. Bartholomew *et al.*, 2010; Sole *et al.*, 2011; Sundal *et al.*, 2011; Banwell *et al.*, 2013, 2016; Chandler *et al.*, 2013; Andrews *et al.*, 2014). Therefore, by  
580 including these rapidly draining small lakes, the FASTER algorithm with the dual-satellite record could be used to provide a better dataset than previously for the testing of lake-~~filling and~~ ~~draining~~ models (e.g. Banwell *et al.*, 2012; Arnold *et al.*, 2014), or alternatively to specify the input locations and water volumes for the forcing of subglacial-~~hydrology~~ models with much greater confidence than would be possible with MODIS alone. Further work is still required, however, to determine  
585 whether the water volumes delivered by these small lakes during the drainage process are capable of temporarily pressurising the subglacial drainage system, such that ice velocity speed-up events may occur, and to determine whether the associated deviations from background stresses in the far field would be enough sufficient to open moulins outside the basins of small lakes or to trigger chain-reaction-style rapid lake drainage (cf. Christoffersen *et al.*, 2018; Hoffman *et al.*, 2018).

Over the 2016 ~~summer melt season~~, 27% of all lakes detected in the region drained rapidly, compared with 21% that drained  
590 rapidly in 2014 across the slightly smaller Paakitsoq region contained within the region of this study (Williamson *et al.*, 2017). However, that earlier study used MODIS imagery, so it omitted the rapid drainage of small lakes, which could explain the lower percentage if it is assumed that these small lakes are more likely to drain rapidly than the large ones, relative to the total numbers of lakes in each category. ~~The~~ Our 27% value in this study compares well with that of 22% from Miles *et al.* (2017), who also tracked changes to small lakes using a similar tracking threshold to that used here, albeit for a different combination  
595 of satellite platforms (Landsat 8 and Sentinel-1), and for a larger region of West Greenland in summer 2015. ~~Finally,~~ The ~~error precision of a~~ rapid lake-drainage dates in this study ( $\pm 1.1$  days) is ~~smaller~~ higher than that identified by Miles *et al.* (2017) ( $\pm 4.0$  days); this likely results from the different temporal resolution of Sentinel-1 compared with Sentinel-2, and because Miles *et al.* (2017) were forced to discard some images before conducting their analysis, reducing the average temporal resolution and so the ability to identify rapid lake drainage dates confidently. Thus, although Sentinel-1 can image through  
600 clouds, the Sentinel-1 record suffers from separate issues that offset this advantage. The shorter time interval for repeat lake imaging offered by the FASTER algorithm is likely to help reduce the observation bias associated with the longer time intervals

of existing remote-sensing (e.g. MODIS-based) work (Cooley and Christoffersen, 2017). We also offer an ~~additional~~ advance ~~over their~~ with the dual-satellite method since we can calculate the water volumes delivered into the GrIS by rapid lake drainage (because of the use of using optical satellite data), in addition to the lake-area changes that could be tracked previously (e.g. Miles et al., 2017). ~~whereas Miles et al.'s (2017) study could only identify lake area changes using the Landsat 8 and Sentinel-1 combination.~~

## 5 Conclusions

We have presented the results of the first approach to combine two medium-resolution optical satellite datasets (Sentinel-2 and Landsat 8) to generate the highest spatial- and temporal-resolution record of lake area and volume evolution on the GrIS to date. To achieve this, we have exploited the increasing availability of medium- to high-resolution satellite imagery, and then combined these newly available data with recent techniques for automatically tracking changes to lake areas and volumes, and for identifying rapid lake drainage. The resultant FASTER algorithm allows lake areas and volumes to be calculated with high accuracy from Sentinel-2. For lake area, the RMSE is 0.007 km<sup>2</sup> when compared with that derived from Landsat 8 data, which is nearly fifty times lower than the error associated with MODIS. For lake depth, the RMSE is 0.555 m, under half that associated with MODIS. The techniques for lake-~~area~~ and lake-depth calculation from Sentinel-2, when combined with similar techniques applied to Landsat 8 data, yielded a dual-satellite record with comparable temporal resolution (2.8 days) to that of MODIS (daily). Thus, the FASTER algorithm applied here reduces the large errors associated with calculating lake depth and ~~to a lesser extent,~~ lake area using the ancestral FAST algorithm applied to the coarser spatial resolution MODIS imagery (Williamson *et al.*, 2017). In addition, the FASTER algorithm provides a similarly frequent site revisit time as MODIS, allowing rapid lake drainage to be identified with ~~low error~~ high precision ( $\pm 1.1$  days). Our work shows that using both sets of high-resolution satellite imagery together provides better insights into lake filling and drainage than using either one in isolation. With the availability of Sentinel-2B data from summer 2017 to supplement the Sentinel-2A data used in this study, the three datasets could be used together to generate an even higher temporal resolution record. In the future, the dual-satellite record presented here is therefore likely to be able to replace, or at least supplement, the MODIS record used to investigate lakes on the GrIS.

We have additionally taken advantage of new, and increasingly reliable, downscaled regional climate-model (RACMO2.3p2) output data (Noël *et al.*, 2018) to provide insights into the volumes of ~~surface meltwater runoff~~ entering the GrIS's englacial or subglacial hydrological systems after moulin opening was identified using the FASTER algorithm. Our results show that the water volumes released into the GrIS by small lakes during the lake-drainage events themselves are small (only 5.1%) relative to the volumes released by all lake-drainage events, suggesting small lakes are less ~~not~~ important in this sense. However, of the total water volume that subsequently reaches the GrIS's internal hydrological system ~~interior~~ via all moulins opened ~~up~~ by lake drainage (from both large and small lakes), moulins opened ~~up~~ by small lakes deliver 61.5% of the total water volume. This suggests that small lakes are important to include in future remote-sensing and modelling studies.

Resulting from the above, the FASTER algorithm holds great potential for generating novel insights into lake behaviour on the GrIS from remote sensing, including for small lakes that change quickly (cf. Miles *et al.*, 2017). Future work should focus on applying the FASTER algorithm to wider areas of the GrIS and comparing the results with increasingly available and reliable high temporal resolution ice-velocity data (e.g. Joughin *et al.*, 2018) to investigate the influence of lake drainage on the observed patterns of intra- and inter-annual velocity variations across the GrIS. Moreover, the high spatial resolution record could be used to identify the potential controls on the initiation of rapid lake drainage, something that could not be achieved with MODIS data, perhaps due to the data's coarse spatial resolution (Williamson *et al.*, 2018). Finally, the water volumes delivered into the GrIS during the rapid lake-drainage events identified with this record, the moulins that are assumed to open

during such events, and the subsequent runoff that enters the GrIS via these moulins, could be used as forcing or testing data for subglacial-hydrology models (e.g. Hewitt, 2013; Banwell *et al.*, 2016) and linked hydrology-ice dynamics models (e.g. Koziol and Arnold, 2018). Ultimately, applications of the FASTER algorithm such as these could enable the GrIS's supraglacial and subglacial hydrology to be modelled more accurately in order to provide better constraints on future runoff, ice discharge and sea-level rise from the GrIS.

*Data availability.* All ~~S~~satellite imagery and regional climate-model ~~output~~ data used in the analysis are ~~freely available open access.~~ ~~AGW can distribute~~ ~~†~~The full MATLAB source code for the FASTER algorithm used to process and analyse the imagery to other researchers is freely available for download (Williamson, 2018b).

*Author contributions.* AGW conceived the study, designed and executed the method presented in the research, conducted the analysis, and drafted the original manuscript, all under the supervision of the other authors. All authors discussed the results and contributed towards editing the manuscript. AGW responded to reviewer comments and revised the manuscript.

*Competing interests.* The authors declare that they have no conflict of interest.

*Acknowledgements.* AGW was funded by a UK Natural Environment Research Council PhD studentship (NE/L002507/1) awarded through the Cambridge Earth System Science Doctoral Training Partnership and a Cambridge Philosophical Society Research Studentship. AFB was funded by a Leverhulme/Newton Trust Early Career Fellowship (ECF-2014-412). The Scott Polar Research Institute's B. B. Roberts Fund and the Cambridge Philosophical Society provided funding for AGW to present this research at the European Geosciences Union General Assembly 2018. We are grateful to Allen Pope for discussing the results of the Sentinel-2 lake-depth calculations with us, and to Brice Noël for speedily providing the RACMO2.3p2 data. Katie Miles and Corinne Benedek are thanked for generally contributing to the idea for the study, and we thank Gareth Rees and Pete Nienow for providing thoughtful feedback on this work. Finally, detailed reviewer comments from Allen Pope, Samuel Doyle and Kristin Poinar helped to significantly improve the quality of the manuscript.

## References

- Andrews, L. C., Catania, G. A., Hoffman, M. J., Gulley, J. D., Lüthi, M. P., Ryser, C., Hawley, R. L., and Neumann, T. A.: Direct observations of evolving subglacial drainage beneath the Greenland Ice Sheet, *Nature*, 514, 80–83, <https://doi.org/10.1038/nature13796>, 2014.
- Arnold, N. S., Banwell, A. F., and Willis, I. C.: High-resolution modelling of the seasonal evolution of surface water storage on the Greenland Ice Sheet, *The Cryosphere*, 8, 1149–1160, <https://doi.org/10.5194/tc-8-1149-2014>, 2014.
- Banwell, A. F., Arnold, N. S., Willis, I. C., Tedesco, M., and Ahlstrøm, A. P.: Modeling supraglacial water routing and lake filling on the Greenland Ice Sheet, *J. Geophys. Res.-Earth*, 117, F04012, <https://doi.org/10.1029/2012JF002393>, 2012.
- Banwell, A. F., Willis, I. C., and Arnold, N. S.: Modeling subglacial water routing at Paakitsoq, W Greenland, *J. Geophys. Res.-Earth*, 118, 1282–1295, <https://doi.org/10.1002/jgrf.20093>, 2013.
- Banwell, A. F., Caballero, M., Arnold, N. S., Glasser, N. F., Cathles, L. M., and MacAyeal, D. R.: Supraglacial lakes on the Larsen B ice shelf, Antarctica, and at Paakitsoq, West Greenland: a comparative study, *Ann. Glaciol.*, 55, 1–8, <https://doi.org/10.3189/2014AoG66A049>, 2014.
- Banwell, A., Hewitt, I., Willis, I., and Arnold, N.: Moulin density controls drainage development beneath the Greenland ice sheet, *J. Geophys. Res.-Earth*, 121, 2248–2269, <https://doi.org/10.1002/2015jf003801>, 2016.
- Bartholomew, I., Nienow, P., Mair, D., Hubbard, A., King, M. A., and Sole, A.: Seasonal evolution of subglacial drainage and acceleration in a Greenland outlet glacier, *Nat. Geosci.*, 3, 408–411, <https://doi.org/10.1038/ngeo863>, 2010.

- 680 Bartholomew, I. D., Nienow, P., Sole, A., Mair, D., Cowton, T., King, M. A., and Palmer, S.: Seasonal variations in Greenland Ice Sheet motion: Inland extent and behaviour at higher elevations, *Earth Planet. Sci. Lett.*, 307, 271–278, <https://doi.org/10.1016/j.epsl.2011.04.014>, 2011a.
- Bartholomew, I., Nienow, P., Sole, A., Mair, D., Cowton, T., Palmer, S., and Wadham, J.: Supraglacial forcing of subglacial drainage in the ablation zone of the Greenland ice sheet, *Geophys. Res. Lett.*, 38, L08502, <https://doi.org/10.1029/2011GL047063>, 2011b.
- 685 Bartholomew, I., Nienow, P., Sole, A., Mair, D., Cowton, T., and King, M. A.: Short-term variability in Greenland Ice Sheet motion forced by time-varying meltwater drainage: Implications for the relationship between subglacial drainage system behavior and ice velocity, *J. Geophys. Res.-Earth*, 117, F03002, <https://doi.org/10.1029/2011jff002220>, 2012.
- Bougamont, M., Christoffersen, P., Hubbard, A. L., Fitzpatrick, A. A., Doyle, S. H., and Carter, S. P.: Sensitive response of the Greenland Ice Sheet to surface melt drainage over a soft bed, *Nat. Comm.*, 5, <https://doi.org/10.1038/ncomms6052>, 2014.
- 690 Box, J. E. and Ski, K.: Remote sounding of Greenland supraglacial melt lakes: implications for subglacial hydraulics, *J. Glaciol.*, 53, 257–265, <https://doi.org/10.3189/172756507782202883>, 2007.
- Chen, C., Howat, I. M., and de la Peña, S.: Formation and development of supraglacial lakes in the percolation zone of the Greenland ice sheet, *J. Glaciol.*, 63, 847–853, <https://doi.org/10.1017/jog.2017.50>, 2017.
- 695 [Christoffersen, P., Bougamont, M., Hubbard, A., Doyle, S. H., Grigsby, S., and Pettersson, R.: Cascading lake drainage on the Greenland Ice Sheet triggered by tensile shock and fracture, \*Nat. Commun.\*, 9, 1064, <https://doi.org/10.1038/s41467-018-03420-8>, 2018.](https://doi.org/10.1038/s41467-018-03420-8)
- Chu, V.: Greenland ice sheet hydrology: A review, *Prog. Phys. Geog.*, 38, 19–54, <https://doi.org/10.1177/0309133313507075>, 2014.
- 700 Colgan, W., Steffen, K., McLamb, W. S., Abdalati, W., Rajaram, H., Motyka, R., Phillips, T., and Anderson, R.: An increase in crevasse extent, West Greenland: Hydrologic implications, *Geophys. Res. Lett.*, 38, L18503, <https://doi.org/10.1029/2011GL048491>, 2011.
- [Cooley, S. W. and Christoffersen, P.: Observation bias correction reveals more rapidly draining lakes on the Greenland Ice Sheet, \*J. Geophys. Res.-Earth\*, 122, 1867–1881, <https://doi.org/10.1002/2017JF004255>, 2017.](https://doi.org/10.1002/2017JF004255)
- 705 Cowton, T., Nienow, P., Sole, A., Wadham, J., Lis, G., Bartholomew, I., Mair, D., and Chandler, D.: Evolution of drainage system morphology at a land-terminating Greenlandic outlet glacier, *J. Geophys. Res.-Earth*, 118, 29–41, <https://doi.org/10.1029/2012jff002540>, 2013.
- Das, S. B., Joughin, I., Behn, M. D., Howat, I. M., King, M. A., Lizarralde, D., and Bhatia, M. P.: Fracture propagation to the base of the Greenland Ice Sheet during supraglacial lake drainage, *Science*, 320, 778–781, <https://doi.org/10.1126/science.1153360>, 2008.
- de Fleurian, B., Morlighem, M., Seroussi, H., Rignot, E., van den Broeke, M. R., Munneke, P. K., Mouginot, J., Smeets, P. C. J. P., and Tedstone, A. J.: A modeling study of the effect of runoff variability on the effective pressure beneath Russell Glacier, West Greenland, *J. Geophys. Res.-Earth*, 121, 1834–1848, <https://doi.org/10.1002/2016JF003842>, 2016.
- 715 Dow, C. F., Kulesa, B., Rutt, I. C., Doyle, S. H., and Hubbard, A.: Upper bounds on subglacial channel development for interior regions of the Greenland ice sheet, *J. Glaciol.*, 60, 1044–1052, <https://doi.org/10.3189/2014JoG14J093>, 2014.
- Doyle, S. H., Hubbard, A. L., Dow C. F., Jones, G. A., Fitzpatrick, A., Gusmeroli, A., Kulesa, B., Lingback, K., Pettersson, R., and Box, J. E.: Ice tectonic deformation during the rapid in situ drainage of a supraglacial lake on the Greenland Ice Sheet, *The Cryosphere*, 7, 129–140, <https://doi.org/10.5194/tc-7-129-2013>, 2013.
- 720 Doyle, S. H., Hubbard, A., Fitzpatrick, A. A. W., van As, D., Mikkelsen, A. B., Pettersson, R., and Hubbard, B.: Persistent flow acceleration within the interior of the Greenland ice sheet, *Geophys. Res. Lett.*, 41, 899–905, <https://doi.org/10.1002/2013GL058933>, 2014.

- 725 Doyle, S. H., Hubbard, B., Christoffersen, P., Young, T. J., Hofstede, C., Bougamont, M., Box, J. E., and Hubbard, A.: Physical conditions of fast glacier flow: 1. Measurements from boreholes drilled to the bed of Store Glacier, West Greenland, *J. Geophys. Res.-Earth*, 123, <https://doi.org/10.1002/2017JF004529>, 2018.
- Everett, A., Murray, T., Selmes, N., Rutt, I. C., Luckman, A., James, T. D., Clason, C., O'Leary, M., Karunarathna, H., Moloney, V., and Reeve, D. E.: Annual down-glacier drainage of lakes and water-filled crevasses at Helheim Glacier, southeast Greenland, *J. Geophys. Res.-Earth*, 121, 1819–1833, <https://doi.org/10.1002/2016JF003831>, 2016.
- 730 Feng, L. and Hu, C.: Cloud adjacency effects on top-of-atmosphere radiance and ocean color data products: A statistical assessment, *Remote Sens. Environ.*, 174, 301–313, <https://doi.org/10.1016/j.rse.2015.12.020>, 2016.
- Fitzpatrick, A. A. W., Hubbard, A., Joughin, I., Quincey, D. J., van As, D., Mikkelsen, A. P. B., Doyle, S. H., Hasholt, B., and Jones, G. A.: Ice flow dynamics and surface meltwater flux at a land-terminating sector of the Greenland ice sheet, *J. Glaciol.*, 59, 687–696, <https://doi.org/10.3189/2013JoG12J143>, 2013.
- 735 Fitzpatrick, A. A. W., Hubbard, A. L., Box, J. E., Quincey, D. J., van As, D., Mikkelsen, A. P. B., Doyle, S. H., Dow, C. F., Hasholt, B., and Jones, G. A.: A decade (2002–2012) of supraglacial lake volume estimates across Russell Glacier, west Greenland, *The Cryosphere*, 8, 107–121, <https://doi.org/10.5194/tc-8-107-2014>, 2014.
- Georgiou, S., Shepherd, A., McMillan, M., and Nienow, P.: Seasonal evolution of supraglacial lake volume from ASTER imagery, *Ann. Glaciol.*, 50, 95–100, <https://doi.org/10.3189/172756409789624328>, 2009.
- 740 Gledhill, L. A. and Williamson, A. G.: Inland advance of supraglacial lakes in north-west Greenland under three decades of climate change, *Ann. Glaciol.*, <https://doi.org/10.1017/aog.2017.31>, [1–17](https://doi.org/10.1017/aog.2017.31), 2018.
- Hewitt, I. J.: Seasonal changes in ice sheet motion due to melt water lubrication, *Earth Planet. Sci. Lett.*, 371–372, 16–25, <https://doi.org/10.1016/j.epsl.2013.04.022>, 2013.
- Hock, R., Hutchings, J. K., and Lehning, M.: Grand challenges in cryospheric sciences: Toward better predictability of glaciers, snow and sea ice, *Front. Earth Sci.*, 5, 1–14, <https://doi.org/10.3389/feart.2017.00064>, 2017.
- 745 Hoffman, M. J., Catania, G. A., Neumann, T. A., Andrews, L. C., and Rumrill, J. A.: Links between acceleration, melting, and supraglacial lake drainage of the western Greenland Ice Sheet, *J. Geophys. Res.-Earth*, 116, <https://doi.org/10.1029/2010JF001934>, 2011.
- Hoffman, M. J., Andrews, L. C., Price, S. F., Catania, G. A., Neumann, T. A., Lüthi, M. P., Gulley, J., Ryser, C., Hawley, R. L., and Morriss, B.: Greenland subglacial drainage evolution regulated by weakly connected regions of the bed, *Nat. Comm.*, 7, 13903, <https://doi.org/10.1038/ncomms13903>, 2016.
- 750 Hoffman, M. J., Perego, M., Andrews, L. C., Price, S. F., Neumann, T. A., Johnson, J., Catania, G., and Lüthi, M.: Widespread moulin formation during supraglacial lake drainages in Greenland, *Geophys. Res. Lett.*, 45, <https://doi.org/10.1002/2017GL075659>, 2018.
- 755 Hofstede, C., Christoffersen, P., Hubbard, B., Doyle, S. H., Young, T. J., Diez, A., Eisen, O., and Hubbard, A.: Physical conditions of fast glacier flow: 2. Variable extent of anisotropic ice and soft basal sediment from seismic reflection data acquired on Store Glacier, West Greenland, *J. Geophys. Res.-Earth*, 123, <https://doi.org/10.1002/2017JF004297>, 2018.
- Houborg, R. and McCabe, M. F.: Impacts of dust aerosol and adjacency effects on the accuracy of Landsat 8 and RapidEye surface reflectances, *Remote Sens. Environ.*, 194, 127–145, <https://doi.org/10.1016/j.rse.2017.03.013>, 2017.
- 760 Howat, I. M., Negrete, A., and Smith, B. E.: The Greenland Ice Mapping Project (GIMP) land classification and surface elevation data sets, *The Cryosphere*, 8, 1509–1518, <https://doi.org/10.5194/tc-8-1509-2014>, 2014.
- Johansson, A. M. and Brown, I. A.: Adaptive Classification of Supra-Glacial Lakes on the West Greenland Ice Sheet, *IEEE J. Sel. Top. Appl.*, 6, 1998–2007, <https://doi.org/10.1109/JSTARS.2012.2233722>, 2013.
- Johansson, A. M., Jansson, P., and Brown, I. A.: Spatial and temporal variations in lakes on the Greenland Ice Sheet, *J. Hydrol.*, 476, 314–320, <https://doi.org/10.1016/j.jhydrol.2012.10.045>, 2013.

- 765 Joughin, I., Das, S. B., King, M. A., Smith, B. E., Howat, I. M., and Moon, T.: Seasonal speedup along the western flank of the Greenland Ice Sheet, *Science*, 320, 781–783, <https://doi.org/10.1126/science.1153288>, 2008.
- [Joughin, I., Das, S. B., Flowers, G. E., Behn, M. D., Alley, R. B., King, M. A., Smith, B. E., Bamber, J. L., van den Broeke, M. R., and van Angelen, J. H.: Influence of ice-sheet geometry and supraglacial lakes on seasonal ice-flow variability, \*The Cryosphere\*, 7, 1185–1192, <https://doi.org/10.5194/tc-7-1185-2013>, 2013.](#)
- 770 Joughin, I., Smith, B. E., Howat, I. M., Moon, T., and Scambos, T.: A SAR record of early 21st century change in Greenland, *J. Glaciol.*, 62, 62–71, <https://doi.org/10.1017/jog.2016.10>, 2016.
- Joughin, I., Smith, B. E., and Howat, I. M.: A complete map of Greenland ice velocity derived from satellite data collected over 20 years, *J. Glaciol.*, 64, 1–11, <https://doi.org/10.1017/jog.2017.73>, 2018.
- Kääb, A., Winsvold, S. H., Altena, B., Nuth, C., Nagler, T., and Wuite, J.: Glacier remote sensing using Sentinel-2. Part I: Radiometric and geometric performance, and application to ice velocity, *Remote Sens.*, 8, 598, <https://doi.org/10.3390/rs8070598>, 2016.
- 775 Kjeldsen, K. K., Khan, S. A., Bjørk, A. A., Nielsen, K., and Mouginot, J.: Ice-dammed lake drainage in west Greenland: Drainage pattern and implications on ice flow and bedrock motion, *Geophys. Res. Lett.*, 44, 7320–7327, <https://doi.org/10.1002/2017GL074081>, 2017.
- 780 Koziol, C. P. and Arnold, N.: Modelling seasonal meltwater forcing of the velocity of the Greenland Ice Sheet, *The Cryosphere*, 12, 971–991, <https://doi.org/10.5194/tc-2017-225>, 2018.
- Koziol, C., Arnold, N., Pope, A., and Colgan, W.: Quantifying supraglacial meltwater pathways in the Paakitsoq region, West Greenland, *J. Glaciol.*, 63, 464–476, <https://doi.org/10.1017/jog.2017.5>, 2017.
- Krawczynski, M. J., Behn, M. D., Das, S. B., and Joughin, I.: Constraints on the lake volume required for hydro-fracture through ice sheets, *Geophys. Res. Lett.*, 36, L10501, <https://doi.org/10.1029/2008GL036765>, 2009.
- 785 Kulesa, B., Hubbard, A. L., Booth, A. D., Bougamont, M., Dow, C. F., Doyle, S. H., Christoffersen, P., Lindbäck, K., Petterson, R., Fitzpatrick, A. A. W., and Jones, G. A.: Seismic evidence for complex sedimentary control of Greenland Ice Sheet flow, *Sci. Adv.*, 3, 1–8, <https://doi.org/10.1126/sciadv.1603071>, 2017.
- Leeson, A. A., Shepherd, A., Palmer, S., Sundal, A., and Fettweis, X.: Simulating the growth of supraglacial lakes at the western margin of the Greenland ice sheet, *The Cryosphere*, 6, 1077–1086, <https://doi.org/10.5194/tc-6-1077-2012>, 2012.
- 790 Leeson, A. A., Shepherd, A., Sundal, A. V., Johansson, A. M., Selmes, N., Briggs, K., Hogg, A. E., and Fettweis, X.: A comparison of supraglacial lake observations derived from MODIS imagery at the western margin of the Greenland ice sheet, *J. Glaciol.*, 59, 1179–1188, <https://doi.org/10.3189/2013JoG13J064>, 2013.
- Legleiter, C. J., Tedesco, M., Smith, L. C., Behar, A. E., and Overstreet, B. T.: Mapping the bathymetry of supraglacial lakes and streams on the Greenland ice sheet using field measurements and high-resolution satellite images, *The Cryosphere*, 8, 215–228, <https://doi.org/10.5194/tc-8-215-2014>, 2014.
- 795 Lüthi, M. P., Ryser, C., Andrews, L. C., Catania, G. A., Funk, M., Hawley, R. L., Hoffman, M. J., and Neumann, T. A.: Heat sources within the Greenland Ice Sheet: dissipation, temperature paleo-firn and cryo-hydrologic warming, *The Cryosphere*, 9, 245–253, <https://doi.org/10.5194/tc-9-245-2015>, 2015.
- 800 Lüthje, M., Pedersen, L. T., Reeh, N., and Greuell, W.: Modelling the evolution of supraglacial lakes on the West Greenland ice-sheet margin, *J. Glaciol.*, 52, 608–618, <https://doi.org/10.3189/172756506781828386>, 2006.
- Macdonald, G. J., Banwell, A. F., and MacAyeal, D. R.: Seasonal evolution of supraglacial lakes on a floating ice tongue, Petermann Glacier, Greenland, *Ann. Glaciol.*, <https://doi.org/10.1017/aog.2018.9>, 1–10, [in press 2018](#).
- Mankoff, K. D. and Tulaczyk, S. M.: The past, present and future viscous heat dissipation available for Greenland subglacial conduit formation, *The Cryosphere*, 11, 303–317, <https://doi.org/10.5194/tc-11-303-2017>, 2017.
- 805 McMillan, M., Nienow, P., Shepherd, A., Benham, T., and Sole, A.: Seasonal evolution of supra-glacial lakes on the Greenland Ice Sheet, *Earth Planet. Sci. Lett.*, 262, 484–492, <https://doi.org/10.1016/j.epsl.2007.08.002>, 2007.

- Miles, K. E., Willis, I. C., Benedek, C. L., Williamson, A. G., and Tedesco, M.: Toward monitoring surface and subsurface lakes on the Greenland Ice Sheet using Sentinel-1 SAR and Landsat 8 OLI imagery, *Front. Earth Sci.*, 5, 1–17, <https://doi.org/10.3389/feart.2017.00058>, 2017.
- Morriss, B. F., Hawley, R. L., Chipman, J. W., Andrews, L. C., Catania, G. A., Hoffman, M. J., Lüthi, M. P., and Neumann, T.: A ten-year record of supraglacial lake evolution and rapid drainage in West Greenland using an automated processing algorithm for multispectral imagery, *The Cryosphere*, 7, 1869–1877, <https://doi.org/10.5194/tc-7-1869-2013>, 2013.
- Moussavi, M. S., Abdalati, W., Pope, A., Scambos, T., Tedesco, M., MacFerrin, M., and Grigsby, S.: Derivation and validation of supraglacial lake volumes on the Greenland Ice Sheet from high-resolution satellite imagery, *Remote Sens. Environ.*, 183, 294–303, <https://doi.org/10.1016/j.rse.2016.05.024>, 2016.
- Naegeli, K., Damm, A., Huss, M., Wulf, H., Schaepman, M., and Hoelzle, M.: Cross-comparison of albedo products for glacier surfaces derived from airborne and satellite (Sentinel-2 and Landsat 8) optical data, *Remote Sens.*, 9, 110, <https://doi.org/10.3390/rs9020110>, 2017.
- Nienow, P. W., Sole, A. J., Slater, D. A., and Cowton, T. R.: Recent advances in our understanding of the role of meltwater in the Greenland ice sheet system, *Curr. Clim. Change Rep.*, 3, <https://doi.org/10.1007/s40641-017-0083-9>, 2017.
- Noël, B., van de Berg, W. J., van Wessem, J. M., van Meijgaard, E., van As, D., Lenaerts, J. T. M., Lhermitte, S., Kuipers Munneke, P., Smeets, C. J. P. P., van Ulft, L. H., van de Wal, R. S. W., and van den Broeke, M. R.: Modelling the climate and surface mass balance of polar ice sheets using RACMO2 – Part 1: Greenland (1958–2016), *The Cryosphere*, [12](https://doi.org/10.5194/tc-12-811-2018), 811–831, <https://doi.org/10.5194/tc-12-811-2018>, 2018.
- Palmer, S., Shepherd, A., Nienow, P., and Joughin, I.: Seasonal speedup of the Greenland Ice Sheet linked to routing of surface water, *Earth Planet. Sci. Lett.*, 302, 423–428, <https://doi.org/10.1016/j.epsl.2010.12.037>, 2011.
- Paul, F., Winsvold, S. H., Käab, A., Nagler, T., and Schwaizer, G.: Glacier remote sensing using Sentinel-2. Part II: Mapping glacier extents and surface facies, and comparison to Landsat 8, *Remote Sens.*, 8, 575, <https://doi.org/10.3390/rs8070575>, 2016.
- Phillips, T., Rajaram, H., and Steffen, K.: Cryo-hydrologic warming: A potential mechanism for rapid thermal response of ice sheets, *Geophys. Res. Lett.*, 37, <https://doi.org/10.1029/2010GL044397>, 2010.
- Phillips, T., Rajaram, H., Colgan, W., Steffen, K., and Abdalati, W.: Evaluation of cryo-hydrologic warming as an explanation for increased ice velocities in the wet snow zone, Sermeq Avannarleq, West Greenland, *J. Geophys. Res.-Earth*, 118, 1241–1256, <https://doi.org/10.1002/jgrf.20079>, 2013.
- Poinar, K., Joughin, I., Das, S. B., Behn, M. D., Lenaerts, J., and van den Broeke, M. R.: Limits to future expansion of surface-melt-enhanced ice flow into the interior of western Greenland, *Geophys. Res. Lett.*, 42, 1800–1807, <https://doi.org/10.1002/2015GL063192>, 2015.
- Poinar, K., Joughin, I., Lenaerts, J. T. M., and van den Broeke, M. R.: Englacial latent-heat transfer has limited influence on seaward ice flux in western Greenland, *J. Glaciol.*, 63, 1–16, <https://doi.org/10.1017/jog.2016.103>, 2017.
- Pope, A.: Reproducibly estimating and evaluating supraglacial lake depth with Landsat 8 and other multispectral sensors, *Earth Space Sci.*, 3, 176–188, <https://doi.org/10.1002/2015EA000125>, 2016.
- Pope, A., Scambos, T. A., Moussavi, M., Tedesco, M., Willis, M., Shean, D., and Grigsby, S.: Estimating supraglacial lake depth in West Greenland using Landsat 8 and comparison with other multispectral sensors, *The Cryosphere*, 10, 15–27, <https://doi.org/10.5194/tc-10-15-2016>, 2016.
- Schoof, C.: Ice-sheet acceleration driven by melt supply variability, *Nature*, 468, 803–806, <https://doi.org/10.1038/nature09618>, 2010.
- Selmes, N., Murray, T., and James, T. D.: Fast draining lakes on the Greenland Ice Sheet, *Geophys. Res. Lett.*, 38, L15501, <https://doi.org/10.1029/2011GL047872>, 2011.

- 850 Selmes, N., Murray, T., and James, T. D.: Characterizing supraglacial lake drainage and freezing on the Greenland Ice Sheet, *The Cryosphere Discuss.*, 7, 475–505, <https://doi.org/10.5194/tcd-7-475-2013>, 2013.
- Shepherd, A., Hubbard, A., Nienow, P., King, M., McMillan, M., and Joughin, I.: Greenland ice sheet motion coupled with daily melting in late summer, *Geophys. Res. Lett.*, 36, L01501, <https://doi.org/10.1029/2008GL035758>, 2009.
- Sneed, W. A. and Hamilton, G. S.: Evolution of melt pond volume on the surface of the Greenland Ice Sheet, *Geophys. Res. Lett.*, 34, L03501, <https://doi.org/10.1029/2006GL028697>, 2007.
- 855 Sole, A., Mair, D. W. F., Nienow, P. W., Bartholomew, I. D., King, M. A., Burke, M. J., and Joughin, I.: Seasonal speedup of a Greenland marine-terminating outlet glacier forced by surface melt-induced changes in subglacial hydrology, *J. Geophys. Res.-Earth*, 116, <https://doi.org/10.1029/2010JF001948>, 2011.
- Sole, A., Nienow, P., Bartholomew, I., Mair, D., Cowton, T., Tedstone, A., and King, M. A.: Winter motion mediates dynamic response of the Greenland Ice Sheet to warmer summers, *Geophys. Res. Lett.*, 40, 3940–3944, <https://doi.org/10.1002/grl.50764>, 2013.
- 860 Stevens, L. A., Behn, M. D., McGuire, J. J., Das, S. B., Joughin, I., Herring, T., Shean, D. E., and King, M. A.: Greenland supraglacial lake drainages triggered by hydrologically induced basal slip, *Nature*, 522, 73–76, <https://doi.org/10.1038/nature14608>, 2015.
- 865 Stevens, L. A., Behn, M. D., Das, S. B., Joughin, I., Noël, B. P. Y., van den Broeke, M., and Herring, T.: Greenland Ice Sheet flow response to runoff variability, *Geophys. Res. Lett.*, 43, 11,295–11,303, <https://doi.org/10.1002/2016GL070414>, 2016.
- Sundal, A. V., Shepherd, A., Nienow, P., Hanna, E., Palmer, S., and Huybrechts, P.: Evolution of supra-glacial lakes across the Greenland Ice Sheet, *Remote Sens. Environ.*, 113, 2164–2171, <https://doi.org/10.1016/j.rse.2009.05.018>, 2009.
- Sundal, A. V., Shepherd, A., Nienow, P., Hanna, E., Palmer, S. and Huybrechts, P.: Melt-induced speed-up of Greenland ice sheet offset by efficient subglacial drainage, *Nature*, 469, 521–524, <https://doi.org/10.1038/nature09740>, 2011.
- 870 Tedesco, M., Lüthje, M., Steffen, K., Steiner, N., Fettweis, X., Willis, I., Bayou, N., and Banwell, A.: Measurement and modeling of ablation of the bottom of supraglacial lakes in western Greenland, *Geophys. Res. Lett.*, 39, L02052, <https://doi.org/10.1029/2011GL049882>, 2012.
- Tedesco, M., Willis, I. C., Hoffman, M. J., Banwell, A. F., Alexander, P., and Arnold, N. S.: Ice dynamic response to two modes of surface lake drainage on the Greenland ice sheet, *Environ. Res. Lett.*, 8, 034007, <https://doi.org/10.1088/1748-9326/8/3/034007>, 2013.
- 875 Tedstone, A. J., Nienow, P. W., Gourmelen, N. and Sole, A. J.: Greenland ice sheet annual motion insensitive to spatial variations in subglacial hydraulic structure, *Geophys. Res. Lett.*, 41, 8910–8917, <https://doi.org/10.1002/2014GL062386>, 2014.
- 880 Tedstone, A. J., Nienow, P. W., Gourmelen, N., Dehecq, A., Goldberg, D., and Hanna, E.: Decadal slowdown of a land-terminating sector of the Greenland Ice Sheet despite warming, *Nature*, 526, 692–695, <https://doi.org/10.1038/nature15722>, 2015.
- van de Wal, R. S. W., Boot, M., van den Broeke, M. R., Smeets, C. J. P. P., Reijmer, C. H., Donker, J. J. A., and Oerlemans, J.: Large and rapid melt-induced velocity changes in the ablation zone of the Greenland Ice Sheet, *Science*, 321, 111–113, <https://doi.org/10.1126/science.1158540>, 2008.
- 885 van de Wal, R. S. W., Smeets, C. J. P. P., Boot, W., Stoffelen, M., van Kampen, R., Doyle, S. H., Wilhelms, F., van den Broeke, M. R., Reijmer, C. H., Oerlemans, J., and Hubbard, A.: Self-regulation of ice flow varies across the ablation area in south-west Greenland, *The Cryosphere*, 9, 603–611, <https://doi.org/10.5194/tc-9-603-2015>, 2015.
- van den Broeke, M. R., Enderlin, E. M., Howat, I. M., Kuipers Munneke, P., Noël, B. P. Y., van de Berg, W. J., van Meijgaard, E., and Wouters, B.: On the recent contribution of the Greenland ice sheet to sea level change, *The Cryosphere*, 10, 1933–1946, <https://doi.org/10.5194/tc-10-1933-2016>, 2016.
- 890

[Williamson, A. G.: Remote sensing of rapidly draining supraglacial lakes on the Greenland Ice Sheet, PhD thesis, University of Cambridge, Cambridge, UK, https://doi.org/10.17863/CAM.24192, 2018a.](https://doi.org/10.17863/CAM.24192)

[Williamson, A.: Full source code for the Fully Automated Supraglacial lake Tracking at Enhanced Resolution \(“FASTER”\) algorithm, version 1 \[software\], https://doi.org/10.17863/CAM.25769, 2018b.](https://doi.org/10.17863/CAM.25769)

895

Williamson, A. G., Arnold, N. S., Banwell, A. F., and Willis, I. C.: A Fully Automated Supraglacial lake area and volume Tracking (“FAST”) algorithm: Development and application using MODIS imagery of West Greenland, *Remote Sens. Environ.*, 196, 113–133, <https://doi.org/10.1016/j.rse.2017.04.032>, 2017.

Williamson, A. G., Willis, I. C., Arnold, N. S., and Banwell, A. F.: Controls on rapid supraglacial lake drainage in West Greenland: an Exploratory Data Analysis approach, *J. Glaciol.*, **64**, 208–226, <https://doi.org/10.1017/JoG.2018.8>, 2018.

900

Zwally, H. J., Abdalati, W., Herring, T., Larson, K., Saba, J., and Steffen, K.: Surface melt-induced acceleration of Greenland ice-sheet flow, *Science*, 297, 218–222, <https://doi.org/10.1126/science.1072708>, 2002.

## S1 Calculating the values of $g$

We followed the methods of Pope *et al.* (2016; their Supplement) to calculate ~~the value for~~ the coefficient for the losses in upward and downward travel through the water column ( $g$ ;  $\text{m}^{-1}$ ) for the red and green bands of Sentinel-2. The relationship from Smith and Baker (1981; their Eq. (5)) states that:

$$K_d = a + \frac{1}{2}b, \quad (\text{S1})$$

where  $K_d$  is the diffuse attenuation coefficient for the clearest natural freshwaters,  $a$  is the absorption coefficient for pure water, and  $b$  is the backscattering coefficient for molecular (Rayleigh) scattering in freshwater.

We then used the relationship from Sneed and Hamilton (2007; their Eq. (3)), which indicates that:

$$g \approx K_d + aD_u, \quad (\text{S2})$$

where  $D_u$  is an upwelling light distribution or the reciprocal of the upwelling average cosine (Mobley, 1994). Since  $K_d \approx aD_u$  (Maritorena *et al.*, 1994),  $g$  can simply be calculated (using measured values of  $a$  and  $b$ ) with the following:

$$g = 2(K_d), \quad (\text{S3})$$

meaning that Eq. (S1) could then be used to derive the following relationship:

$$g = 2(a + \frac{1}{2}b). \quad (\text{S4})$$

For  $a$ , we followed Pope *et al.* (2016) and took the value from Pope and Fry (1997; their Table 3) to replace that from Smith and Baker (1981; their Table 1), and, for  $b$ , we took the value from Buiteveld *et al.* (1994; their Table 1) for each wavelength of Sentinel-2's red and green bands. This allowed a preliminary  $g$  value to be calculated for each of Sentinel-2's red and green bands by using Eq. (S4) for each wavelength of the red band (from 646–684 nm in 1 nm increments) and green band (from 537–582 nm in 1 nm increments). To derive ~~a~~ final  $g$  values for each band, following Pope *et al.* (2016), Sentinel-2's spectral response function (ESA, 2017) was used ~~akin to the data available for Landsat 8 (Barsi *et al.*, 2014)), and ~~an~~ average weighted values were ~~were~~ calculated according to the spectral response for each wavelength of the red and green bands.~~

This produced ~~a~~ final  $g$  values for Sentinel-2's red band of 0.8304 and for Sentinel-2's green band of 0.1413, which compared ~~s~~ with the lower  $g$  values for Landsat 8's red band of 0.7507 and for Landsat 8's green band of 0.1279 (Pope *et al.*, 2016).

**Table S1:** Details of Sentinel-2 Multispectral Instrument images used in the study. Cloud cover was determined from the image metadata, representing the percentage of cloud-covered pixels both within the ice-sheet area and off the ice-sheet edge. Data cover was determined from the image metadata, representing the percentage of the total area of the region (i.e. the area on the ice sheet plus the ice-marginal area) for which satellite data were collected.

| Scene ID  | UTM zone | Latitude band | Square | Date   | Year | Sequence | Cloud cover (%) | Data cover (%) |
|---|----------|---------------|--------|--------|------|----------|-----------------|----------------|
| S2A_OPER_MSI_L1C_DS_MTI_20160502T202602_S20160502T151916_N02.01 | 22N      | W             | EC     | 02 May | 2016 | 0        | 38.9            | 100.0          |
| S2A_OPER_MSI_L1C_DS_SGS_20160505T205541_S20160505T152915_N02.02 | 22N      | W             | EC     | 05 May | 2016 | 0        | 44.7            | 100.0          |
| S2A_OPER_MSI_L1C_DS_MTI_20160515T203516_S20160515T152912_N02.02 | 22N      | W             | EC     | 15 May | 2016 | 0        | 5.4             | 100.0          |
| S2A_OPER_MSI_L1C_DS_SGS_20160518T210306_S20160518T154153_N02.02 | 22N      | W             | EC     | 18 May | 2016 | 0        | 31.4            | 38.3           |
| S2A_OPER_MSI_L1C_DS_MTI_20160522T202416_S20160522T151915_N02.02 | 22N      | W             | EC     | 22 May | 2016 | 0        | 29.8            | 100.0          |
| S2A_OPER_MSI_L1C_DS_MTI_20160529T201543_S20160529T150918_N02.02 | 22N      | W             | EC     | 29 May | 2016 | 0        | 66.1            | 94.3           |
| S2A_OPER_MSI_L1C_DS_SGS_20160601T173946_S20160601T151916_N02.02 | 22N      | W             | EC     | 01 Jun | 2016 | 0        | 18.1            | 99.9           |
| S2A_OPER_MSI_L1C_DS_MTI_20160604T203539_S20160604T152915_N02.02 | 22N      | W             | EC     | 04 Jun | 2016 | 0        | 60.0            | 99.9           |
| S2A_OPER_MSI_L1C_DS_SGS_20160608T202646_S20160608T150916_N02.02 | 22N      | W             | EC     | 08 Jun | 2016 | 0        | 16.2            | 94.2           |
| S2A_OPER_MSI_L1C_DS_MTI_20160611T202435_S20160611T151937_N02.02 | 22N      | W             | EC     | 11 Jun | 2016 | 0        | 42.5            | 100.0          |
| S2A_OPER_MSI_L1C_DS_SGS_20160617T192017_S20160617T153910_N02.04 | 22N      | W             | EC     | 17 Jun | 2016 | 0        | 25.7            | 38.9           |
| S2A_OPER_MSI_L1C_DS_SGS_20160618T202441_S20160618T151305_N02.04 | 22N      | W             | EC     | 18 Jun | 2016 | 0        | 46.7            | 93.2           |
| S2A_OPER_MSI_L1C_DS_MTI_20160621T220258_S20160621T151912_N02.04 | 22N      | W             | EC     | 21 Jun | 2016 | 0        | 4.3             | 100.0          |
| S2A_OPER_MSI_L1C_DS_MTI_20160624T203434_S20160624T152911_N02.04 | 22N      | W             | EC     | 24 Jun | 2016 | 0        | 16.0            | 100.0          |
| S2A_OPER_MSI_L1C_DS_SGS_20160628T202858_S20160628T150914_N02.04 | 22N      | W             | EC     | 28 Jun | 2016 | 0        | 0.1             | 94.0           |
| S2A_OPER_MSI_L1C_DS_MTI_20160701T202434_S20160701T151913_N02.04 | 22N      | W             | EC     | 01 Jul | 2016 | 0        | 73.3            | 100.0          |
| S2A_OPER_MSI_L1C_DS_SGS_20160707T192822_S20160707T153908_N02.04 | 22N      | W             | EC     | 07 Jul | 2016 | 0        | 0.0             | 38.6           |
| S2A_OPER_MSI_L1C_DS_SGS_20160708T202909_S20160708T151305_N02.04 | 22N      | W             | EC     | 08 Jul | 2016 | 1        | 1.6             | 94.2           |
| S2A_OPER_MSI_L1C_DS_SGS_20160711T203749_S20160711T151912_N02.04 | 22N      | W             | EC     | 11 Jul | 2016 | 0        | 0.1             | 100.0          |
| S2A_OPER_MSI_L1C_DS_MTI_20160714T203553_S20160714T152910_N02.04 | 22N      | W             | EC     | 14 Jul | 2016 | 0        | 0.3             | 99.9           |
| S2A_OPER_MSI_L1C_DS_SGS_20160718T202939_S20160718T150915_N02.04 | 22N      | W             | EC     | 18 Jul | 2016 | 0        | 23.7            | 94.2           |

| Scene ID  | UTM zone | Latitude band | Square | Date   | Year | Sequence | Cloud cover (%) | Data cover (%) |
|---|----------|---------------|--------|--------|------|----------|-----------------|----------------|
| S2A_OPER_MSI_L1C_DS_MTI_20160721T202530_S20160721T151913_N02.04 | 22N      | W             | EC     | 21 Jul | 2016 | 0        | 0.0             | 100.0          |
| S2A_OPER_MSI_L1C_DS_SGS_20160724T205100_S20160724T153051_N02.04 | 22N      | W             | EC     | 24 Jul | 2016 | 0        | 0.0             | 99.9           |
| S2A_OPER_MSI_L1C_DS_SGS_20160727T192945_S20160727T153910_N02.04 | 22N      | W             | EC     | 27 Jul | 2016 | 0        | 0.0             | 38.2           |
| S2A_OPER_MSI_L1C_DS_SGS_20160728T202436_S20160728T151306_N02.04 | 22N      | W             | EC     | 28 Jul | 2016 | 0        | 63.6            | 94.3           |
| S2A_OPER_MSI_L1C_DS_SGS_20160731T203724_S20160731T151913_N02.04 | 22N      | W             | EC     | 31 Jul | 2016 | 0        | 0.0             | 100.0          |
| S2A_OPER_MSI_L1C_DS_MTI_20160803T203554_S20160803T152910_N02.04 | 22N      | W             | EC     | 03 Aug | 2016 | 0        | 3.1             | 100.0          |
| S2A_OPER_MSI_L1C_DS_MTI_20160806T204409_S20160806T153909_N02.04 | 22N      | W             | EC     | 06 Aug | 2016 | 0        | 14.1            | 38.1           |
| S2A_OPER_MSI_L1C_DS_SGS_20160807T202758_S20160807T150914_N02.04 | 22N      | W             | EC     | 07 Aug | 2016 | 0        | 55.9            | 94.4           |
| S2A_OPER_MSI_L1C_DS_MTI_20160810T202535_S20160810T151912_N02.04 | 22N      | W             | EC     | 10 Aug | 2016 | 0        | 13.0            | 100.0          |
| S2A_OPER_MSI_L1C_DS_SGS_20160813T204833_S20160813T153046_N02.04 | 22N      | W             | EC     | 13 Aug | 2016 | 0        | 0.0             | 100.0          |
| S2A_OPER_MSI_L1C_DS_SGS_20160817T202447_S20160817T151257_N02.04 | 22N      | W             | EC     | 17 Aug | 2016 | 0        | 0.7             | 94.4           |
| S2A_OPER_MSI_L1C_DS_MTI_20160830T202522_S20160830T151909_N02.04 | 22N      | W             | EC     | 30 Aug | 2016 | 0        | 2.2             | 100.0          |
| S2A_OPER_MSI_L1C_DS_SGS_20160902T204312_S20160902T153051_N02.04 | 22N      | W             | EC     | 02 Sep | 2016 | 0        | 0.7             | 100.0          |
| S2A_OPER_MSI_L1C_DS_SGS_20160906T202733_S20160906T151257_N02.04 | 22N      | W             | EC     | 06 Sep | 2016 | 0        | 35.9            | 94.5           |
| S2A_OPER_MSI_L1C_DS_SGS_20160909T203815_S20160909T151907_N02.04 | 22N      | W             | EC     | 09 Sep | 2016 | 0        | 21.0            | 100.0          |
| S2A_OPER_MSI_L1C_DS_MTI_20160912T203709_S20160912T152817_N02.04 | 22N      | W             | EC     | 12 Sep | 2016 | 0        | 0.0             | 100.0          |
| S2A_OPER_MSI_L1C_DS_SGS_20160915T210159_S20160915T154130_N02.04 | 22N      | W             | EC     | 15 Sep | 2016 | 0        | 1.7             | 38.2           |
| S2A_OPER_MSI_L1C_DS_MTI_20160926T201345_S20160926T150955_N02.04 | 22N      | W             | EC     | 26 Sep | 2016 | 0        | 0.3             | 93.9           |

**Table S2:** Details of Landsat 8 Operational Land Imager images used in the study. Cloud cover was calculated as the percentage of pixels both on and off the ice sheet that were obscured by clouds (i.e. those with a band-6 [or SWIR](#) value > 0.100; Sect. 2.2.1). Data cover was calculated as a percentage of the total area of the region (i.e. the area on the ice sheet plus the ice-marginal area) for which satellite data had been collected. [\\*The asterisk](#) denotes that the image was used for comparing lake areas calculated from the two satellites and for validating the lake depths from Sentinel-2, but that the image was not used for lake tracking because a contemporaneous higher-resolution, and therefore more favourable, Sentinel-2 image was available.

| Scene ID              | Path | Row | Date    | Year | Cloud cover (%) | Data cover (%) |
|-----------------------|------|-----|---------|------|-----------------|----------------|
| LC80100112016149LGN01 | 010  | 011 | 28 May  | 2016 | 85.9            | 95.1           |
| LC80080112016151LGN01 | 008  | 011 | 30 May  | 2016 | 8.4             | 72.8           |
| LC80822332016157LGN01 | 082  | 233 | 05 Jun  | 2016 | 17.3            | 100.0          |
| LC80090112016158LGN01 | 009  | 011 | 06 Jun  | 2016 | 21.6            | 100.0          |
| LC80100112016165LGN01 | 010  | 011 | 13 Jun  | 2016 | 43.9            | 95.3           |
| LC80090112016174LGN01 | 009  | 011 | 22 Jun  | 2016 | 33.9            | 100.0          |
| LC80100112016181LGN01 | 010  | 011 | 29 Jun  | 2016 | 35.0            | 95.2           |
| LC80080112016183LGN01 | 008  | 011 | 01 Jul* | 2016 | 60.8            | 72.6           |
| LC80100112016197LGN01 | 010  | 011 | 15 Jul  | 2016 | 21.0            | 95.1           |
| LC80812332016198LGN01 | 081  | 233 | 16 Jul  | 2016 | 19.0            | 93.7           |
| LC80080112016199LGN01 | 008  | 011 | 17 Jul  | 2016 | 5.9             | 72.8           |
| LC80100112016213LGN01 | 010  | 011 | 31 Jul* | 2016 | 18.5            | 95.2           |
| LC80080112016215LGN01 | 008  | 011 | 02 Aug  | 2016 | 12.2            | 72.6           |
| LC80090112016222LGN01 | 009  | 011 | 09 Aug  | 2016 | 18.4            | 100.0          |
| LC80100112016229LGN01 | 010  | 011 | 16 Aug  | 2016 | 18.3            | 95.2           |
| LC80080112016231LGN01 | 008  | 011 | 18 Aug  | 2016 | 6.5             | 72.7           |
| LC80080112016247LGN01 | 008  | 011 | 03 Sep  | 2016 | 8.8             | 73.2           |

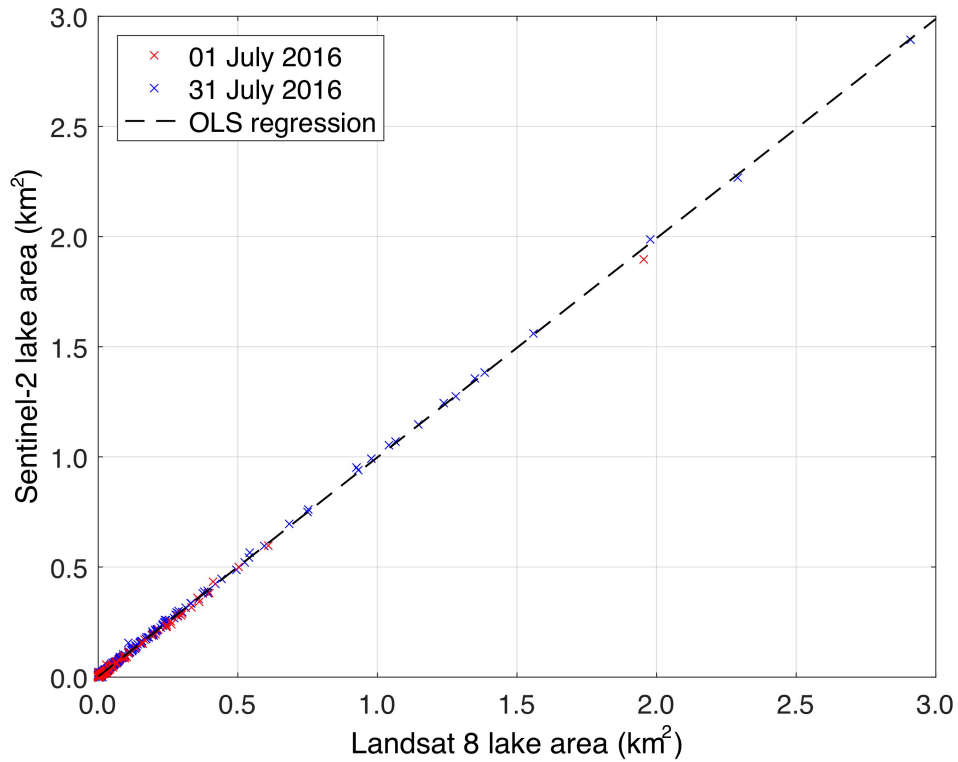


**Figure S1:** The very strong relationship between Landsat 8 and Sentinel-2 lake areas for the days of overlapping imagery (1 July and 31 July) in 2016. The 594 lake areas used for comparisons were derived using the Normalised Difference Water Index (NDWI) approach with threshold values of 0.25 for both types of imagery. The black dashed line shows an ordinary least-squares (OLS) linear regression, which can explain 99.9% ( $R^2 = 0.999$ ;  $p = 0.000$ ) of the variance in the data. The root-mean square error of  $0.007 \text{ km}^2$  (i.e. seven Sentinel-2 pixels) between the two sets of lake areas is [therefore](#) remarkably small.

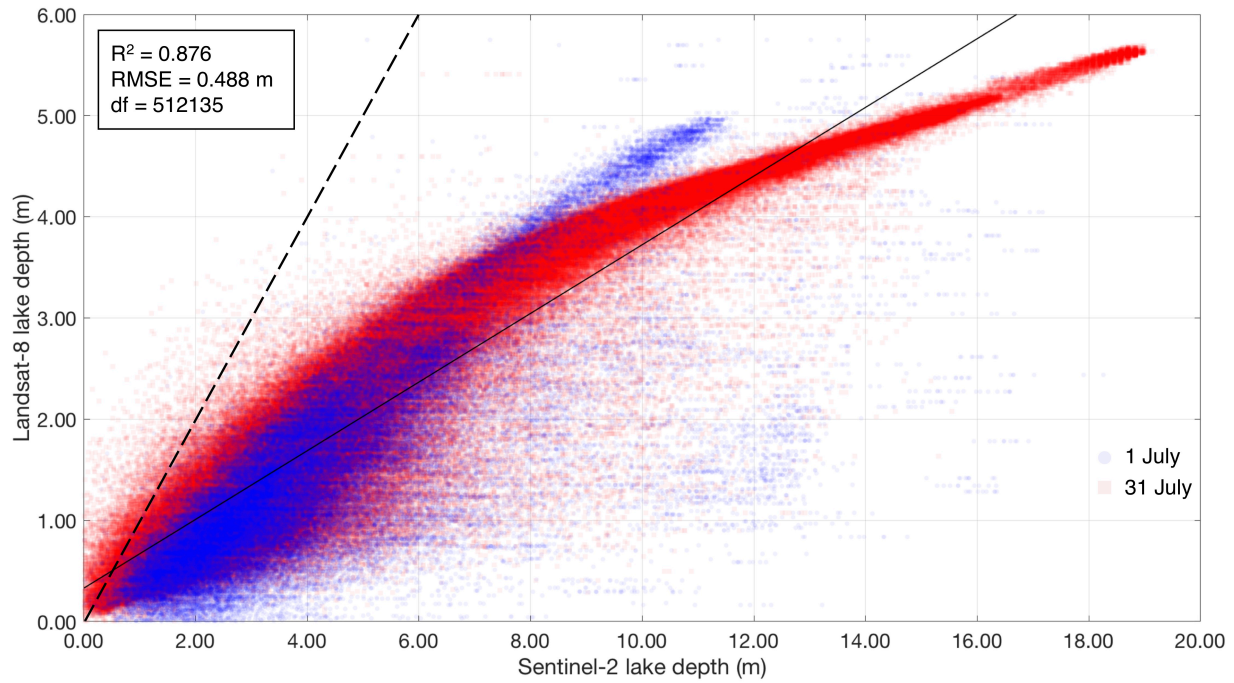


**Figure S2:** Comparison of lake depths calculated using the physically based method for Sentinel-2 (with the green band) and for Landsat 8 (with the average depths from the red and panchromatic bands). Degrees of freedom (“df” in this figure) = 512,135. The solid black line shows an ordinary least-squares (OLS) linear regression and the dashed black line shows a 1:1 relation. The  $R^2$  value indicates that the regression explains 87.6% of the variance in the data. The RMSE of 0.488 m shows the error associated with calculating the Sentinel-2 lake depths using this relationship.

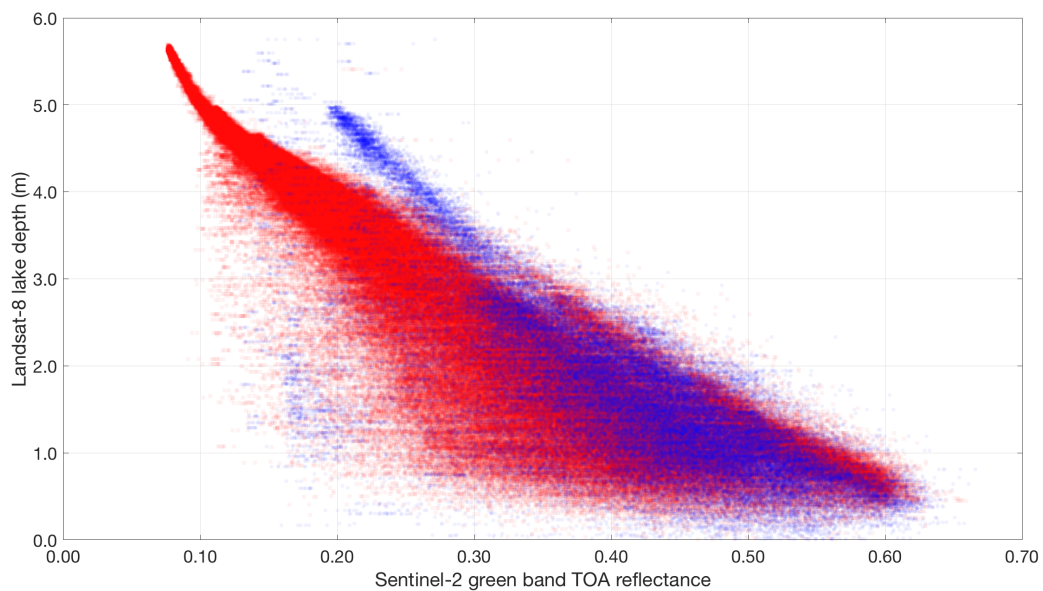


**Figure S3:** Scatter plot to show the relationship between Sentinel-2 green band top-of-atmosphere (TOA) reflectance and Landsat 8 lake depth for 430,650 data points (blue circles markers = 1 July; red squares markers = 31 July).

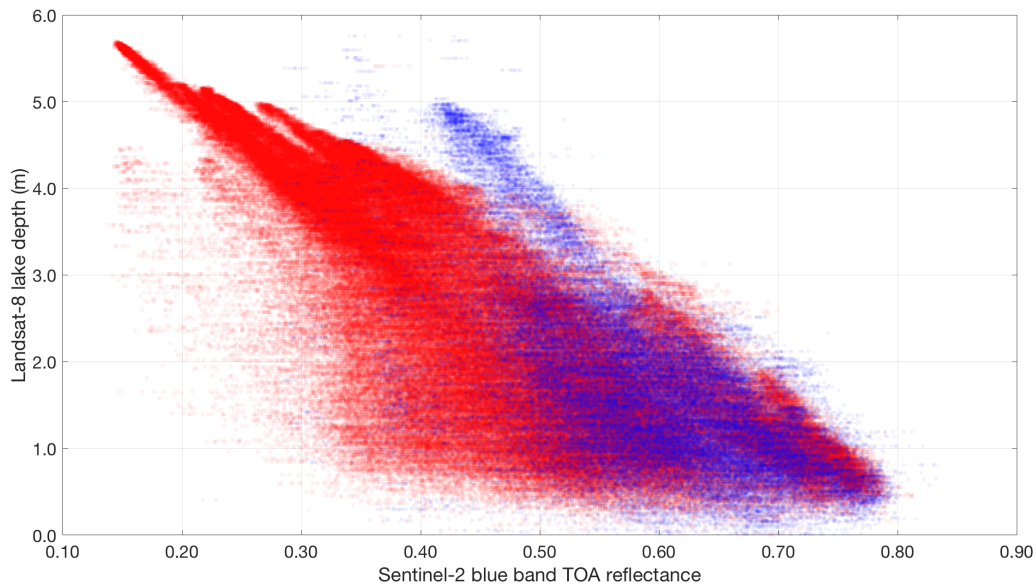


**Figure S43:** Scatter plot to show the relationship between Sentinel-2 blue band TOA reflectance and Landsat 8 lake depth for 430,650 data points (blue circles markers = 1 July; red markers squares = 31 July).

## References

- Barsi, J. A., Lee, K., Kvaran, G., Markham, B. L., and Pedelty, J. A.: The spectral response of the Landsat-8 Operational Land Imager, *Remote Sens.*, 6, 10232–10251, <https://doi.org/10.3390/rs61010232>, 2014.
- ESA: Sentinel-2 spectral response functions (S2-SRF), accessed 19 February 2018, [https://earth.esa.int/web/sentinel/user-guides/sentinel-2-msi/document-library/-/asset\\_publisher/Wk0TKajiISaR/content/sentinel-2a-spectral-responses](https://earth.esa.int/web/sentinel/user-guides/sentinel-2-msi/document-library/-/asset_publisher/Wk0TKajiISaR/content/sentinel-2a-spectral-responses), 2017.
- Maritorena, S., Morel, A., and Gentili, B.: Diffuse reflectance of oceanic shallow waters: Influence of water depth and bottom albedo, *Limnol. Oceanogr.*, 39, 1689–1703, <https://doi.org/10.4319/lo.1994.39.7.1689>, 1994.
- Mobley, C. D.: *Light and water: Radiative transfer in natural waters*, Academic Press, San Diego, 1994.
- Pope, A., Scambos, T. A., Moussavi, M., Tedesco, M., Willis, M., Shean, D., and Grigsby, S.: Estimating supraglacial lake depth in West Greenland using Landsat 8 and comparison with other multispectral sensors, *The Cryosphere*, 10, 15–27, <https://doi.org/10.5194/tc-10-15-2016>, 2016.
- Pope, R. M. and Fry, E. S.: Absorption spectrum (380–700 nm) of pure water. II. Integrating cavity measurements, *Appl. Opt.*, 36, 8710–8723, <https://doi.org/10.1364/AO.36.008710>, 1997.
- Smith, R. C. and Baker, K. S.: Optical properties of the clearest natural waters (200–800 nm), *Appl. Opt.*, 20, 177–184, <https://doi.org/10.1364/AO.20.000177>, 1981.
- Sneed, W. A. and Hamilton, G. S.: Evolution of melt pond volume on the surface of the Greenland Ice Sheet, *Geophys. Res. Lett.*, 34, L03501, <https://doi.org/10.1029/2006GL028697>, 2007.